EFFECT OF BASE CAVITIES ON THE DRAG AND WAKE OF A TWO-DIMENSIONAL BLUFF BODY

BY

ARAVIND CHANDRAMOHAN
(ABDURRAHMAAN)

A Thesis Presented to the

DEANSHIP OF GRADUATE STUDIES

KING FAHD UNIVERSITY OF PETROLEUM & MINERALS

DHAHRAN, SAUDI ARABIA

In Partial Fulfillment of the
Requirements for the Degree of

MASTER OF SCIENCE

In

AEROSPACE ENGINEERING

APRIL 2009

KING FAHD UNIVERSITY OF PETROLEUM & MINERALS
DHAHRAN 31261, SAUDI ARABIA

DEANSHIP OF GRADUATE STUDIES

This thesis, written by **ARAVIND CHANDRAMOHAN (ABDURRAHMAAN)** under the direction of his thesis advisor and approved by his thesis committee, has been presented to and accepted by Dean of Graduate Studies, in partial fulfillment of the requirements for the degree of MASTER OF SCIENCE IN **AEROSPACE ENGINEERING**.

Thesis Committee

Dr. Abdullah M. Al-Garni (Advisor)

Dr. Ahmed Z. Al-Garni (Co-Advisor)

Dr. Ayman H. Kassem (Member)

Dr. Wael G. Abdelrahman (Member)

Dr. Maged A.I. El-Shaarawi (Member)

7/5/1430 H.

Dr. Ahmed Z. Al-Garni 2/5/2009 G.
(Department Chairman)

Dr. Salam A. Zummo
(Dean of Graduate Studies)

2/5/09 [Date]

This work is dedicated to
my beloved
parents, wife and brother-in-laws.

ACKNOWLEDGMENTS

All praise and thanks are due to Almighty Allah, Most Gracious and Most Merciful, for his immense beneficence and blessings. He gave me the extra-ordinary patience to bear the hardships and carry out the work which has resulted in the accomplishment of this research. May peace and blessings be upon prophet Muhammad (PBUH), his family and his companions.

I would like to acknowledge K F U P M for the support extended towards my research through its remarkable facilities and for providing me with the opportunity to pursue graduate studies.

I am indebted to my thesis advisor Dr. Abdullah M. Al-Garni for his help, support, valuable suggestions and timely advice. He was very helpful in getting this work done, and his guidance and encouragement are highly appreciated.

I am also highly grateful to my thesis co-advisor Dr. Ahmed Z. Al-Garni for his constant and consistent, guidance and motivation, inspite of his busy time schedule. His strong support towards this research has always been a boon to me especially during hardships.

Many thanks and appreciation to my thesis committee members, Dr. Ayman H. Kassem, Dr. Wael G. Abdelrahman and Dr. Maged A.I. El-Shaarawi, for their valuable help and advice.

My sincere and heartfelt thanks to my wife and my brother-in-law Mubasshir for their constant motivation and encouragement without which this work would have been very difficult for me to accomplish. Thanks also to my parents who supported me in my efforts. Thanks to Bilal, Irfan, Faisal, Mumtaz, Imran, Owais, Mujahid, Fareed, Misbah, Abdurrahmaan, Mujahid Faiz, Ayub, Ammar, Yusuf, Kabrere, Dr. Ahsan Zafrullah, Aamir, Omer, Masih, Imran Ghani, Muddassir, Sarfaraz, Murtuza, Frazi, Mazhar, Naeem and many others for their help and prayers.

TABLE OF CONTENTS

LIST OF FIGURES

LIST OF TABLES

THESIS ABSTRACT (English)

Name: Aravind Chandramohan (Abdurrahmaan)

Title: Effect of Base Cavities on the Drag and Wake of a Two-Dimensional Bluff Body

Major Field: Aerospace Engineering

Date of Degree: Rabi` Al-Thani 1430 (H) (April 2009 (G)).

In the present investigation, we tested the effects of various cavities on the base drag and wake of a two-dimensional bluff body. The bluff body model has a blunt base and an elliptical leading edge of semimajor to semiminor axis ratio of 8:1. Different lengths and shapes of cavities were attached to the blunt base of the bluff body. Experiments were conducted in the 1×1 m^2 wind tunnel of the Department of Aerospace Engineering at KFUPM at a Reynolds number (Re_h) of $2.6x10^4$. Steady and unsteady base pressure measurements, force measurements as well as Particle Image Velocimetry (PIV) measurements were conducted to study the flow properties. The steady base pressure measurements show that base pressure increases with the attachment of the cavities. The increase was from -0.58 for the base model to -0.52 with 1/6 h cavity, -0.31 with 1/3 h cavity, -0.42 for 2/3 h cavity and -0.46 for angled cavity. The drag-force measurements show that the highest drag reduction is obtained by using 1/3 h cavity (C_d ~ 0.35) compared to the base model (C_d ~ 0.58) followed by 2/3 h cavity (C_d ~ 0.43), angled cavity (C_d ~ 0.48), 1/6 h cavity (C_d ~ 0.52) and closed-C cavity (C_d ~ 0.54). The unsteady base pressure measurements show a dominating peak at a frequency of 11 Hz corresponding to a Strouhal number of 0.07. The frequency of this peak was not altered by cavities, but the energy of the peak increased. The mean velocity fields obtained by using PIV show two recirculation regions behind the base model and cavities. The lengths of the recirculation region were not altered much with the attachment of the cavities.

MASTER OF SCIENCE DEGREE

KING FAHD UNIVERSITY OF PETROLEUM & MINERALS

Dhahran, Saudi Arabia

THESIS ABSTRACT (Arabic)

ملخص الرسالة

الاسم : أرفند شندراموند (عبدالرحمن)

عنوان الرسالة : تأثر التجويفات الخلفية على مقاومة الهواء لجسم ثنائي الأبعاد ذو خلفية ساقطة

التخصص : هندسة الطيران والفضاء

تاريخ التخرج : أبريل 2009

تقدم هذه الرسالة دراسة لتأثير تجويفات مختلفة على مقاومة الهواء لجسم ثنائي الأبعاد ذو خلفية ساقطة ومقدمة بيضاوية الشكل بنسبة الطول إلى الإرتفاع 1:8. تم تجربة عدة أطوال وأشكال من التجويفات المثبتة في نهاية الجسم ،وتم إجراء التجربة في نفق الـهواء التابع لقسم هندسة الطيران والفضاء بجامعة الملك فهد للبترول والمعادن عند رقم رنولدز يساوي $2,6\times10^4$. لقد تم اخذ قياسـات الضغط الثابتة والغير ثابتة ، وقياس قوة مقاومة الهواء بالاضافة الى استخدام تقنية التصويـر الفوتوغرافي لسرعة الجسيمات لدراسة حركة الهواء خلف الجسم والتجويفات المثبتة. لقد أظهرت قياسات الضغط المستقر أن الضغط يزيد مع التجاويف ولكن بنسب مختلفة حيث كانت الزيادة من - 0.58 للجسم بدون تجويف إلى -0.52 للتجويف 6/1 أ، - 0.31 للتجويف 3/1 أ، - 0.42 للتجويف 3/2 أ و - 0.46 للتجويف المائل حيث أن (أ) تمثل إرتفاع الجسم، أما بالنسبة لقياسات القوة المقاومة فقد حقق التجويف 3/1أ أقل مقاومة للهواء بمعامل 0.35 تقريبا مقارنة مع الجسم بدون تجويفات والذي له معامل مقاومة يساوي 0.58، وبالنسبة للتجويفات الأخرى فقد كانت معاملات مقاومتها كالتالي: 0.42 للتجويف 3/2أ، 0.43 للتجويف المائل، 0.52 للتجويف 6/1أ و 0.54 للتجويف المغلق، في حين أن قياسات الضغط الغير مستقره أثبتت وجود ترددات عند 11 هرتزتساوي رقم ستروهل 0.07، هذه الترددات لا تتغير مع تثبيت التجويفات المختلفة ولكن طاقتها تزيد، أما نتائج حركة الهواء خلف الجسم و التجويفات فقد أظهرت وجود منطقتين لدوران الهواء خلف الجسم و أن طولها لا يتغير كثيرا مع تغير أشكال التجويفات.

درجة شهادة الماجستير

جامعة الملك فهد للبترول و المعادن

الظهران ــ المملكة العربية السعودية .

NOMENCLATURE

b	spanwise length of bluff body model, 600 mm
c'_p	pressure coefficient fluctuations
C_d	drag coefficient
C_p	base pressure coefficient
D	total drag of the bluff body (N)
f	pressure fluctuations frequency in the wake region (Hz)
h	height of the bluff body, 50 mm
l	slant length of the angled cavity (mm)
$\bar{l}$	dimensionless length of l/h (0.18)
L_c	cavity length (mm)
p'	pressure fluctuations
P	pressure at the base of the model (N/m^2)
P_0	stagnation pressure (N/m^2)
P_∞	static pressure (N/m^2)
q	dynamic pressure (N/m^2)
Re_h	Reynolds number based on bluff body height
$R_{pp}(\tau)$	pressure fluctuation autocorrelation
St_h	Strouhal number of vortex shedding based on height
U_1	velocity upstream of the model (m/s)
U_2	velocity downstream of the model (m/s)
u_m	Mean horizontal velocity (m/s)
v_m	Mean vertical velocity (m/s)
x_R	recirculation region length (mm)
$\Phi_{pp}(f)$	pressure fluctuation spectrum
ρ	density of air stream (kg/m^3)
τ	autocorrelation time delay (s)

CHAPTER 1

INTRODUCTION

For the past four decades, extensive research has been done to reduce the base drag behind the bluff bodies with blunt base, by both direct and indirect means. This research has been motivated in part by increased fuel prices, increasing driving speeds of the automobiles and dwindling petroleum resources. It has led to significant advances in the understanding of drag reduction mechanisms for blunt trailing-edged bluff bodies. The problem of turbulent base flows and the drag associated with them has been of significant interest in missile and fighter aircraft design, and also in car and truck design. For performance improvement and energy conservation, it is desirable to reduce the base drag of bluff bodies such as bombs, bullets, automobiles, trucks, buses, planetary shapes and the upswept fuselage of some military cargo aircraft. There is a use for a non-axisymmetric afterbody in combat aircraft and missile applications. Base drag, arising from flow separation at the blunt base of a body, can be a sizeable fraction of total drag in the context of projectiles, missiles and afterbodies of fighter aircraft [1, 2]. Estimates indicate that a 40% reduction in the drag would result in a 16% increase in fuel economy for light cars [2]. We also know that drag causes unnecessary fuel consumption and reduces the efficiency of the automotive bluff body. Hence drag needs to be reduced.

Researchers have found that, by increasing the base pressure of the bluff bodies, by effective mixing of the shear layer in the near wake, and by moving the vortex formation far away from the near wake of the bluff body, it is possible to achieve drag reduction through indirect methods. For direct methods of drag reduction, researchers have found that boat tails and cavities of various sizes and shapes can be employed at the trailing edge of the bluff body to reduce drag to a larger extent.

So far, attempts to control the turbulent wake behind a bluff body for drag reduction have been performed mostly for flow over a circular cylinder due to its geometric simplicity. However, for large-scale transportation vehicles such as buses and trucks, the separation point is fixed at the trailing edge due to their blunt shape near the base surface. In this case, the flow near the trailing edge changes suddenly from a flat-plate boundary layer flow to a wake.

The basic approach for base-drag reduction of bluff bodies has been always trying to influence the near wake, by making small changes in the base geometry in such a way that the base pressure is raised [3]. In two-dimensional subsonic flows, any method that increases the base pressure of the bluff bodies consequently reduces the base drag. Some of the drag reduction techniques are: attaching plates at the end of the body, base bleed, ventilated and closed cavity, and trailing edge modifications. Flow over a two-dimensional bluff body with a blunt trailing edge has a fixed separation point at which the flow suddenly changes from a boundary-layer flow to a wake.

1.1 Description of Bluff bodies and Cavities

1.1.1 Bluff bodies:

A Bluff body is defined as a body for which the major contribution to the drag force is due to pressure forces arising from separation of the boundary layer flow adjacent to the surface over the rearward facing part of the body. For example, a body of circular or rectangular cross section is a bluff body, and so is a flat plate or aerofoil inclined at a high angle to the oncoming flow.

The streamlines do not in general follow the surface of a bluff body to aft near the stagnation point, but separated away from the surface somewhere earlier leaving in some cases an extensive region of low-pressure eddying fluid adjacent to the body. The flow around two-dimensional bluff bodies is characterized by the periodic shedding of eddies into wake and by the large scale energy dissipation in the wake giving rise to a very considerable drag penalty.

Bluff bodies are characterized by unsteady velocity fields and by a more or less precocious separation of the boundary layer from their surface. For these bodies, no simplified mathematical treatment is usually possible, and the forces acting on them may be evaluated either from the solution of the complete Navier-Stokes equations or from the results of ad-hoc experiments. Also one might further distinguish between bodies having different “degrees of bluffness”, by referring to the ratio between the cross-flow dimensions of the separated wake and of the body, or to the extent of the body surface immersed in the separated wake. Bluff bodies have drag coefficients that are at least one order of magnitude

greater than streamlined bodies. For example, the drag coefficient of a circular cylinder (a bluff body) of given thickness (diameter) is 15-20 times the drag coefficient of an airfoil (a streamlined body) having the same thickness. Also for a bluff body, separation prevents the occurring of the recompression in the rear part of the body, so that the pressures in this region are considerably smaller than those acting in the front part.

A pair of shear layers that spring from the separation points on such bluff bodies is inherently unstable and they interact to form strong vortices at a regular frequency. These strong vortices induce a low pressure in the near wake, and this low pressure is responsible for the high drag of bluff bodies [2]. For bluff bodies, streamlining is usually not an option for reducing drag, because the bluff shape is often dictated by other constraints [4]. This situation is particularly true for trucks, buses, and most automobiles. For bluff bodies dominated by pressure drag, drag reduction can be achieved by base flow modifications, such as splitting plates, cavities, base bleed, and suction/blowing.

Bluff bodies can be classified into two categories—high and low aspect ratio. The high aspect ratio bluff bodies have large span, relative to characteristic height, and are generally two-dimensional in nature, e.g. classic cylinder in cross flow, or a symmetric airfoil with a thick, blunt trailing edge. Low aspect ratio bluff bodies are characterized by three-dimensionality or axi-symmetry, e.g., spheres, or cylinders of rectangular or circular cross section aligned axially in the flow direction.

1.1.2 Cavities and Boat tails:

Cavities attached to the base of bluff body have been shown to reduce the drag of the bluff body, and they are used as passive methods to reduce drag and vortex shedding. The optimal aspect ratio depends on the boundary layer displacement thickness, for low Reynolds numbers.

A cavity has two predominant flow patterns in an axi-symmetric bluff body [5]. If a cavity is short in the streamwise direction (relative to its depth) the flow will separate from the upstream cavity wall and reattach onto the downstream wall. For cavities long in the streamwise direction (relative to depth), the flow will separate from the upstream wall, reattach to the cavity floor, separate again shortly ahead of the downstream wall, and finally reattach to the downstream wall. A critical cavity length distinguishes the short cavity flow, commonly referred to as open mode flow, from the long closed mode flow. This behavior can occur in both subsonic and supersonic streams.

There are different types of cavities, and some of them are shown in Figure 1.1. These cavities are:

- Open cavity
- Closed cavity
- Angled cavity
- Multi-stepped cavity

The literature survey reveals that there has not been much discussion, about multi-stepped cavities, angled cavities and closed cavities, but numerical and experimental work

with open cavities has been mentioned to a greater extent. Closed cavities have their rear end closed and their front end attached with the bluff body. These were used mostly at the rear end of bluff bodies like passenger cars, vans, tractor trailers, buses etc,. [6]. Angled cavities have rear ends angled with respect to the horizontal plane. Both open and closed cavities are offset from the bluff body in the vertical direction by some length when they are attached to bluff bodies, but angled cavities are not offset vertically from the horizontal surface of the bluff body base when they are attached. Multi-step cavities have steps which move the vortex formation length downstream far away from the bluff body.

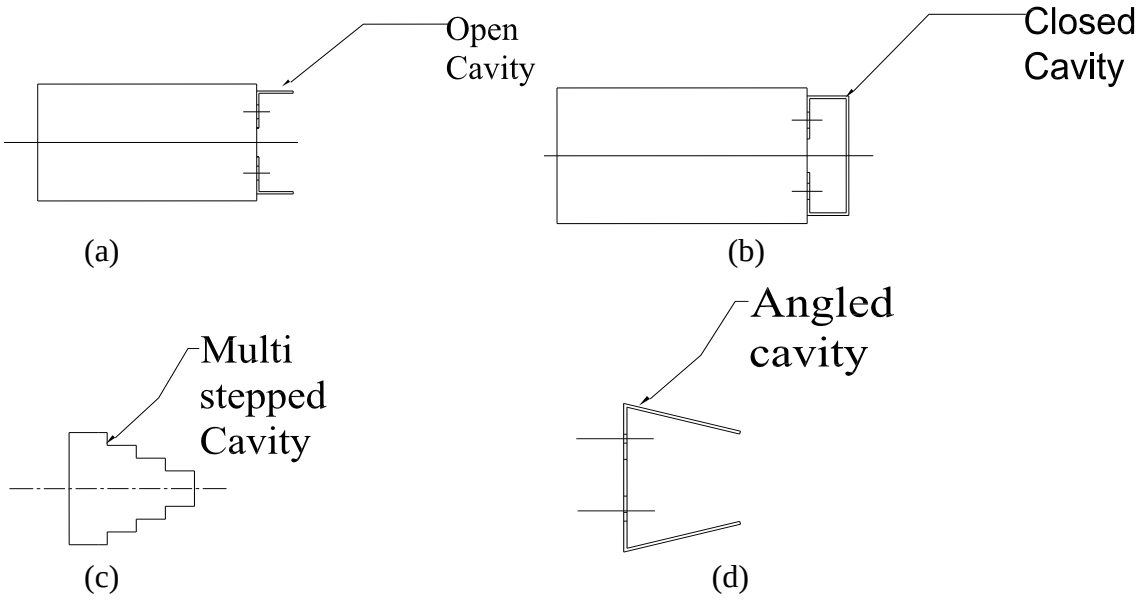

Figure 1.1 Schematic diagram of different types of cavities: (a) Open cavity, (b) Closed cavity, (c) Multi- stepped cavity, and (d) Angled cavity.

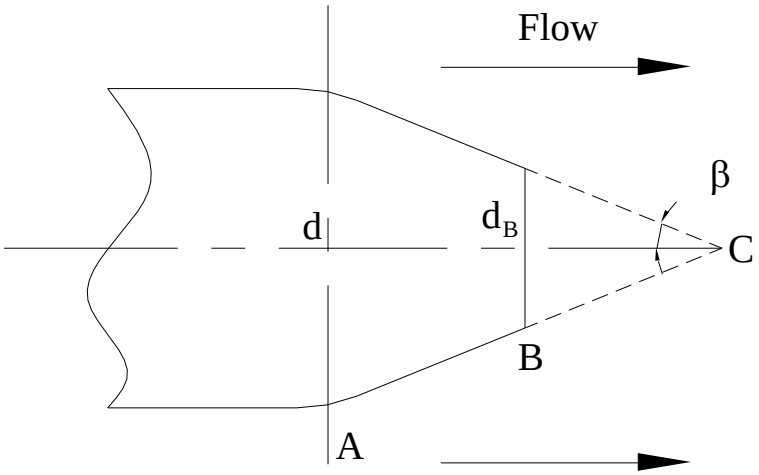

Figure 1.2 Schematic diagram of a boat-tailed afterbody.

It has been known for many years that the drag of a blunt-based body of revolution can be reduced significantly by boat-tailing the rear end in the manner shown in Figure 1.2, [2]. Figure 1.2 refers to a basic body shape consisting of a long cone with a rounded nose, terminating in a blunt base at section B. The portion AB is a typical boat-tailed afterbody, terminating in a blunt base at B with a smaller area than that of the basic body at A. The addition of a further conical body BC, with semi-apex angle β chosen to match the shape of the boat-tailed afterbody at B, would give the "streamline" tail-piece ABC. There is a choice of position for the plane B defining the base of the boat-tailed after-body. The value of the angle β, defining the slope of the boat-tailed after-body at its base B, is a very important variable. If this angle is too large, the boundary layer separates before reaching B. If it is too small, the after-body is unnecessarily long for a given diameter ratio d_B/d, where d is the diameter at A. Earlier research concentrated too much on base drag, and it paid too little attention to the equally important drag force acting on the curved surface AB (in Fig. 1.2).

There was also a tendency to concentrate on circular-arc or straight conical profiles having no rounding at the section A, and this resulted in discontinuity of slope at that section.

Hence a boat-tailed body should be designed in a such a way as to have a cut-off point such that the boundary layer must neither separate upstream of the cut-off point nor delay the separation. Other than this optimal cut-off method, methods employed to delay separation for boundary layer control are vortex generators, suction or blowing.

1.2 Drag Control Methods in the Literature

Control methods have been studied all along for four decades to minimize drag and reduce vortex shedding. We may classify the control methods investigated so far into two groups [8], Homogeneous (Park [8], Wood [9], Yao & Sandham [10]) and Nonhomogeneous in the span wise direction (Tanner [11], Petrusma & Gai [12], Tombazis & Bearman [1]).

In the first approach, a splitter plate (Yao & Sandham [10]) and base bleed (Wood [9], Bearman [13], Yao & Sandham [10]) were used to control the wake behind the blunt-based bluff body for drag reduction. Since the base bleed was applied inside the recirculation region in Wood [9], Bearman [13] and Yao & Sandham [10], a relatively high blowing rate was required for a successful drag reduction. Base suction concentrated near the separation point was also employed as an alternate or additional means of stimulating drag-reducing modifications to the wake, and it is classified as a homogenous control method.

In the Nonhomogeneous approach, the flat base surface of a bluff body was modified into a surface with spanwise modulation. For example, Tanner [11] considered various kinds of spanwise modulation of the trailing edge such as segmented, curved and M-shaped trailing

edges, and examined their drag reduction performances. Petrusma & Gai [12] explored the possibility of drag reduction by using a segmented trailing edge for both laminar and turbulent separating boundary layers, and they determined the optimal geometry of the rectangular segment.

Tombazis and Bearman [1] studied the three-dimensional effects of vortex shedding from a half-ellipse shaped bluff body at a Reynolds number of 2500 and 40,000, based on trailing-edge thickness by using flow visualization techniques. They installed a wavy trailing edge on the blunt-base of the bluff body, and they found that the waviness of the trailing edge produces vortex dislocation in the wake and increases the base pressure. The addition of a wavy trailing edge reduced the base drag, with the largest reductions occurring at peaks in the waves. All these studies revealed that modification of the front or base-surface shape leads to a significant drag reduction. Kim et al. [14] suggested an active open-loop control method (called distributed forcing) for reduction of drag on a two-dimensional bluff body with a blunt trailing edge, where the forcing (blowing and suction) was varied sinusoidally in the spanwise direction, but was steady in time. It was shown that the distributed forcing attenuates the Karman vortex shedding for both laminar and turbulent flows, and thus it reduces the drag significantly.

Hoerner [15,16] suggested that splitter plates increased the base pressure coefficient from -1.3 to -0.8. Later Roshko [17, 18], confirmed that moving the splitter plate downstream from the body would increase the base pressure and decrease the shedding frequency of the periodic vortices. If a long splitter plate was used, the base drag was reduced by half, and the flow reattached to the plate, effectively suppressing the periodicity.

Locked vortex afterbodies were also used in axi-symmetric bluff bodies to reduce drag. Mair [19] was the first who demonstrated that the drag reduction can be achieved by the usage of locked vortex afterbodies in a low speed flow. Also, he demonstrated that the body-disc configuration can experience high drag values (or a drag spike) for a certain combination of diameter of the disc and the spacing, due to the strongly unsteady nature of near-wake flow. This condition is associated with an unstable vortex trapped between the base and the disc which is the judging criterion for drag. The cavity height is also an important factor in determining not only the drag levels, but also the basic characteristics of the flow with a trapped vortex. This combination lead to overall drag reduction of approximately 55% compared to the blunt base. The tail fairing and the boat-tail configurations gave comparable base drag reductions of approximately 70%, which is higher than that of two-disc configuration (approximately 55%).

Multi-stepped afterbodies were also used as drag reduction techniques for bodies of revolution at low speeds. Kentfield [20] pioneered their use in drag reduction. The after bodies were concentric cylinders, making up converging steps if viewed in cross-section. The steps were purported to create captive vortices and to cause the bulk of the flow to converge behind the model. The results for zero-lift drag demonstrated that, while the stepped afterbody offered lower drag compared to the flat base, the boat-tailed base was more effective in reducing the drag further by approximately 20%. This is an important result, since the boat-tailed base had an appreciably larger area than that of the stepped afterbody [21]. The lowest drag reduction achieved for a stepped base was 14 % and it was still 17 % above a truncated boat-tail after-body of the same length and convergence angle [22].

Viswanath [23] proved that, even after optimization of the step geometry, by employing non-uniform step height as well as step length, it was likely that the drag reduction due to attached flow on a properly boat-tailed after-body could not be matched by a stepped after-body.

Viswanath and Patil [24] studied three-dimensional boat-tailed bodies with square and rectangular bases which contain flat segments inclined at a boat-tail angle β to the free stream (assuming zero body incidence) at high speeds. The flow on such an afterbody was very complex, involving three-dimensionality. Interestingly, the boat-tailed body with a square base generated higher base pressure than the axisymmetric counterpart at any given angle β indicating a base drag reduction of approximately 10%. It was comparable to the drag of conical boat-tails, but generally higher than those on the circular arc afterbodies by approximately 10-15%. Conical boat-tails produced higher base pressure in the range of β than did the square-base after-bodies by approximately 2-5%. The after-body drag is the lowest for the circular arc profile resulting from the gradually expanding flow on the boat-tail. Both base and after-body drag levels were much higher for the rectangular base compared to the square base, since the vortices were generally stronger and the low pressure associated with the vortical flow acted over a larger surface area. Not much research has been done on bluff bodies having a square base at transonic and subsonic speeds [24].

The near wake of a two-dimensional bluff body at subsonic Mach numbers and sufficiently high Reynolds numbers is dominated by the periodic and alternate shedding of vortices known as the von-Karman vortex street [25]. These vortices form near the leeward

side or base of the body. The low pressure of the vortex centers is communicated to the base producing a low-base pressure. This combines with the momentum loss associated with the concentration of vorticity to yield an especially high-base drag. This vortex shedding phenomenon is typical of all two-dimensional bluff bodies, and it has great practical importance. Indeed, it is the source of oscillating cross-flow forces that may induce significant oscillations of a structure if their frequency coincides with one of the natural frequencies of the structure.

Park *et al.* [8] further simplified the work of active forcing into a passive device by using tabs as new passive device for the bluff body and also for the backward-facing step [37].

1.3 Previous work

Park *et al*. [8] investigated the effects of small tabs attached to the upper and lower trailing edges on the drag of two-dimensional bluff body by using a wind tunnel and LES. Extensive parametric studies are performed experimentally by varying the height and width of the tab and the spanwise spacing between the adjacent tabs at three Reynolds numbers (Re = 20,000, 40,000 and 80,000). It is found that the base pressure is increased by more than 30% at all Reynolds numbers. The LES computation is performed at much lower Reynolds numbers (Re = 320, 4200). Results from the velocity measurement and numerical simulations show that the tab introduces the spanwise mismatch in the vortex-shedding process, resulting in a substantial reduction of the vortical strength and a significant increase in the vortex formation length and wake width. The area of an optimal tab is much smaller

than the base area of the bluff body, and hence the increase in drag of the tab is very small compared to the decrease in drag of the bluff body. With the optimally configured tabs (i.e. non-staggered multiple tabs) the base pressure is increased over all the spanwise locations by 33% which is larger than that from one pair of tabs (23%). Therefore, the optimally configured multiple tabs, are more effective for reducing drag than one pair of tabs and the staggered multiple tabs, because these tabs effectively attenuate the vortex shedding and reduce the drag. It was concluded that the tab is an effective tool for drag reduction on a two-dimensional bluff body with a blunt trailing edge.

Kim *et al.* [14] studied the reduction of drag on a two-dimensional model vehicle by using the distributed forcing. The forcing (blowing and suction) was applied at the upper and lower trailing edges, and was steady in time but varied sinusoidally in the spanwise direction. Both the large eddy simulation (LES) and the wind-tunnel experiment were carried out at the Reynolds numbers (Re_h) of 4200, 20,000 and 40,000. It was shown by LES (large eddy simulation) that a significant base-pressure recovery (i.e. drag reduction) was obtained with the present distributed forcing, together with a substantial suppression of vortex shedding in the wake behind the model vehicle. Results show that the drag reduction is caused by the direct modification of the vortical structure in the wake rather than by the separation delay. The base pressure is recovered by about 30% with the in-phase distributed forcing over the entire span of the base surface, and hence drag is reduced considerably. It is found that the base pressure is recovered more at the blowing location than at the suction location, because blowing directly prevents the interaction of vortices shed from the upper and lower trailing

edges. Also, the base pressure is nearly unchanged by the out-of phase forcing and rather the base pressure is somewhat increased by the in-phase forcing.

Kruiswyk and Dutton [25] conducted an experimental investigation to study the effects of a base cavity on the near-wake flow field of a slender, two dimensional body in the subsonic speed range (Mach No. 0.4, 0.6 and 0.8). A blunt base, a shallow rectangular cavity base of depth equal to one-half the base height, and a deep rectangular cavity base of depth equal to one base height were the base configurations which were investigated and compared. Each configuration was studied at three free stream Mach numbers, ranging from the low to high subsonic range. The vortex-street was weakened by the base cavity apparently due to the enhanced fluid mixing occurring at the entrance of the cavity, and this yielded higher pressures in the near wake of the cavity bases. The increase in pressure coefficients was in the order of 10-14%, and the increase in shedding frequency was 4-6 % relative to the blunt-based configurations. Structure of the vortex-street was unmodified by the presence of a base cavity. Surface oil flow visualization results proved the 2-dimensionality of the flow. Increasing the depth of the cavity from ½ to 1 base height does not have any significant effect on the parameter being observed. Vortex formation position was pushed slightly further downstream with a base cavity as compared to a blunt base.

Nash [26] made a descriptive review of the previous work on base flow before he published his report, with particular reference to blunt-trailing edge wings. The main factors which influenced base pressure through subsonic and supersonic speeds were discussed in the light of experimental data and current theory.

Nash [27] presented a review of experimental and theoretical research on two-dimensional base flows. This main objective was to illustrate the extent to which the basic properties of the flow are understood in each of the different flow regimes. For the trialing edged cavity geometry, he obtained a reduction in base drag of about 20 % for a 'square' cavity (i.e. of streamwise depth equal to the height of the cavity) and a reduction of 30 % for a cavity which had depth equal to 1-7 times its base height. For ventilated cavity (streamwise slots), it has been found that the edges of the slots act as vortex generators, increasing the mixing in the shear layers. The base pressure was fairly sensitive to the ratio of the length of the slots to the streamwise depth of the cavity in a slotted cavity. Optimum results were obtained when the upstream part of the cavity was solid (about 15 to 20 % of the depth) and the slots covered the remainder. With this configuration, the increase in base pressure was as good as, or better than, that obtained with a splitter plate of length equal to the base height and better than ventilated cavities. It has been demonstrated that, while bleed may be an effective means of eliminating the periodicity, it cannot be considered an economic method for decreasing the base drag. The general conclusion of this work was that combinations of a cavity and a splitter plate were not promising from a practical point of view.

Bearman [28] examined the flow in the wake of a two-dimensional model with a blunt trailing edge at Re = 1.4×10^5 to 2.56×10^5. The ratio of total boundary-layer thickness at the trailing edge to model base height was approximately 0.5. Base pressure and vortex shedding measurements were obtained along the traverse sides of the wake. Results showed a peak in the root mean square velocity-fluctuation at a distance equal to one base height from

the model rear face, which is called the fully formed vortex position. A model fitted with splitter plates was also investigated. For each plate tested, a position of the fully formed vortex was found, and its distance from the model base was discovered to be inversely proportional to the base pressure coefficient. Base pressure dependence on Reynolds number is only between *l*/h=1 to 2 in case of splitter plates, and it becomes independent for *l*/h>2.5 i.e. shedding cease, which indicate that the increase in *l*/h ratio reduces the vortex shedding.

Michael *et al*. [29] used particle image velocimetry (PIV) to study the near-wake structure of a two-dimensional base in subsonic flow and to determine the fluid dynamic mechanisms of base drag reduction in the presence of a base cavity. Experiments were done over a range of free stream Mach numbers up to 0.8, including local flow field velocities over 300 m/s. Effects of the base cavity on the von Karman vortex-street wake were found to be related to the expansion and diffusion of vortices near the cavity. The base cavity effects were also less significant at higher free stream velocities, due to the formation of vortices further downstream from the base. The presence of a solid-walled cavity in the base of a slender two-dimensional body increased the base pressure, resulting in base drag reduction of up to 30%, and it also increased the Strouhal number and the vortex shedding frequency as compared to a blunt base (for cavity depth slightly greater than half the base height). There was diffusion of vortices across the near wake and partially into the cavity, which reduced the strength of vortex motion by 4-6%. The most significant factor affecting the base pressure, and thus the base drag, is the physical displacement of the base surface within the

cavity to a position upstream of the wake where it does not interact with the low-pressure vortices and thus increasing the base pressure and decreasing the base drag.

Viswanath [30] presented a review of the developments that have taken place on the use of passive techniques or devices for axisymmetric base in the absence of jet flow at the base. In particular, the paper discusses the effectiveness of base cavities, ventilated cavities, locked vortex after bodies, multi-step after bodies and afterbodies employing a non-axisymmetric boat-tailing concept for base and net drag reduction in different speed regimes. The broad features of the flow, and the likely fluid-dynamical mechanisms associated with the device leading to base drag reduction, were highlighted. This indicated that base and net after-body drag reduction, which is of considerable engineering significance in aerospace applications, can be achieved by various passive devices, even when the unmanipulated base flow is not characterized by vortex shedding. For non-axisymmetric afterbodies, a square base may have the potential for application in missile and projectile design, as an alternative to the popular conical boat-tail. This work reviewed the developments that took place on the use of passive techniques, devices for axisymmetric and non-axisymmetric base and net after-body drag reduction in different speed regimes. Conical boat-tails were commonly employed on missiles and rockets (non-axisymmetric bodies) which are 3-dimensional in nature. The scope of this review was largely limited to axisymmetric turbulent base flows at zero incidences.

Khalighi *et al.* [31] conducted an experimental and computational investigation of a drag reduction device for bluff bodies in ground proximity. The main goal of this research was to

gain a better understanding of the drag reduction mechanisms in bluff-body square-back geometries. In principle, the device modifies the flow field behind the test model by disturbing the shear layer. The closure of the wake is altered. Unsteady base pressure, hot-wire velocity fluctuations and Particle Image Velocimetry (PIV) measurements of the near wake of the two models (baseline and the modified models) were reported. The drag reduction device suppresses large-scale turbulent motions in the wake, and it reduces the turbulence intensity. The effect of the drag reduction device on the length of the recirculation region in the near wake is small. The boat-tail effect is documented by mean flow streamlines that show the dividing streamlines originating at the tip of the plates, making the recirculation region narrower even though the main recirculation length does not change. Reduction in aerodynamic drag of more than 20%, and the addition of the extension plates, reduces the drag by about 20%. Basically the cavity effect of the Modified Square Back (MSB) model outweighs the adverse pressure effect due to the initial separation from the trailing edge and subsequent reattachment on the extension plate. This cavity effect increases base pressure and reduces base drag.

Mathur and Viswanath [32] carried out experiments in the 0.5-m base flow wind tunnel at high speeds, evaluating the drag reduction potential of a family of square base afterbodies including jet flow at the base. Direct after-body total drag measurements have been made on square bases. The results show conclusively that, in the Mach-number range of 0.95–1.60, the square-base afterbodies have globally minimum drag in the range of jet pressure ratio studied. The total drag reduction observed is about 10–12% relative to the circular arc

afterbodies. Essentially, the flow field is highly viscous dominated and three-dimensional. Results explicitly show that the lowest drag is offered by the square-base after-body, and in particular the drag value of the circular-arc boat tail at β = 8 deg (interpolated) is generally higher than the square base with β = 8 deg. At M_∞ = 0.6, 0.8, and 0.90, the circular-arc after-body has the lowest total drag. At higher M_∞ = 0.95, 1.20, and 1.60, the square-base after-body with β =8 deg has the lowest total drag (10-12% total drag reduction) across the jet pressure ratio in the entire test Mach-number range of this investigation. The flow features on a square-base after-body are quite complex, involving three dimensional vortex flows, but the difference in the validity of the drag data with jet on and off is just 5 %, ensuring the repeatability of the drag data under the same flow conditions.

Pastoor *et al*. [38] examined experimentally and theoretically the drag reduction strategies for the turbulent flow around a D-shaped bluff body at a Reynolds number ranging from 23,000 to 70,000, based on the height of the body. They discussed the effect of open and closed-loop flow control by periodic forcing (suction and blowing), on the coherent structures in the near wake of this body. The derived feedback controller desynchronized the shear-layer and wake dynamics, and postponed the vortex formation. The net energy balance is positive and the invested actuation power is returned by more than four times. This work focused on feedback control for wake stabilization leading to drag reduction. The actuation was applied to only half the span width of the body. Drag reduction of 15% and base pressure increase of 40% with zero-net-mass-flux actuation was achieved.

Cai *et al*. [39] found numerically that shaping the trailing edge of a quasi-streamlined bluff body, in the form of a sinusoidal wave, at a Reynolds number based on base height of 2500, can result in substantial base pressure recovery and drag reduction. The effects of the wavelength of the sinusoidal disturbance on the drag coefficient, vortex shedding mechanism, and frequency selection were examined and compared with previous experimental observations. These results confirm that there is a range of wavelengths where significant drag reduction is possible. A sinusoidal trailing edge, with fixed amplitude and wavelength equal to five times the base height, produces the largest reduction of more than 30% in the mean drag coefficient compared to a straight trailing edge. Lengthening of the mean recirculation region, a substantial drop in the velocity fluctuation at the dominant frequency of the wake, and a relative increase in streamwise vorticity, were observed. The maximum reduction in drag appears to coincide with the transition of the vortex shedding process from a spanwise-irregular to a spanwise-regular mode characterized by spatially well-organized structures along the span.

Beaudoin *et al*. [40] investigated the influence of different flaps located on every edge of the two rear panels of a classic 3D bluff body (very simplified car body) for three freestream velocities 20, 30 and 40 m/s. Flow control was achieved through moving flaps fixed on every edge around the two rear flat surfaces of the model. Different pairs of flaps, with varying angles, were tested. The two most efficient configurations were found to be the two flaps on the side edges of the rear slant and the flap on the top of the rear slant, which gave 17.6% and 15% of drag reduction respectively. The flaps around the base of the model gave 7% drag

reduction. PIV measurements showed that the maximum drag reduction is obtained when the flow is fully separated over the rear slant. i.e. in the region where longitudinal vortices are created.

The conclusions drawn from the literature survey are that:

- Most of the previous studies were done on 2-D axi-symmetric bluff bodies.
- Drag reduction was the ultimate aim of each researcher who worked on the bluff bodies, since it finds its practical applications in the aircraft and automobile industry.
- Drag reduction for a three-dimensional body was tedious and complicated when compared to a two-dimensional body.
- Both passive and active methods, and both homogeneous and non-homogeneous methods, were adopted by the researchers to reduce drag.
- Some of the important objectives of the above research were also to study the effect of drag reduction methods on the vortex shedding and wake separation behind the bluff bodies.

1.4 Present Investigation

The present investigation focuses on the effect of different base cavities on the drag and wake of a two-dimensional bluff body with a blunt trailing edge. Drag reduction of a two-dimensional bluff body with a rectangular base has received little attention in the literature. As mentioned above, most of the previous research focused on axi-symmetric (rounded base) bluff bodies. From the literature review, to our knowledge, no single study

has used the proposed cavities on a 2-D bluff body with an elliptical leading edge. Hence the present investigation will focus on the use of different base cavities other than the ones discussed in the past research to reduce the drag of a 2-D bluff body with an elliptical leading edge.

In the preliminary phase, five different cavities are attached to the base of the bluff body. Steady base pressure and force measurements are conducted to determine the best drag reduction devices. Based on these preliminary measurements, the best three drag reduction cavities will be considered for further investigations. Figure 1.3 (a-c) shows three open cavities with different lengths: 1/6 h, 1/3 h and 2/3 h respectively, where h denotes the height of the bluff body which is 50 mm. Figure 1.3 (d) shows a closed cavity with a length of 1/3 h. The cavity shown in Figure 1.3(e) is an angled cavity of angle 15^{o} from the horizontal plane and with a length of 8.7 mm.

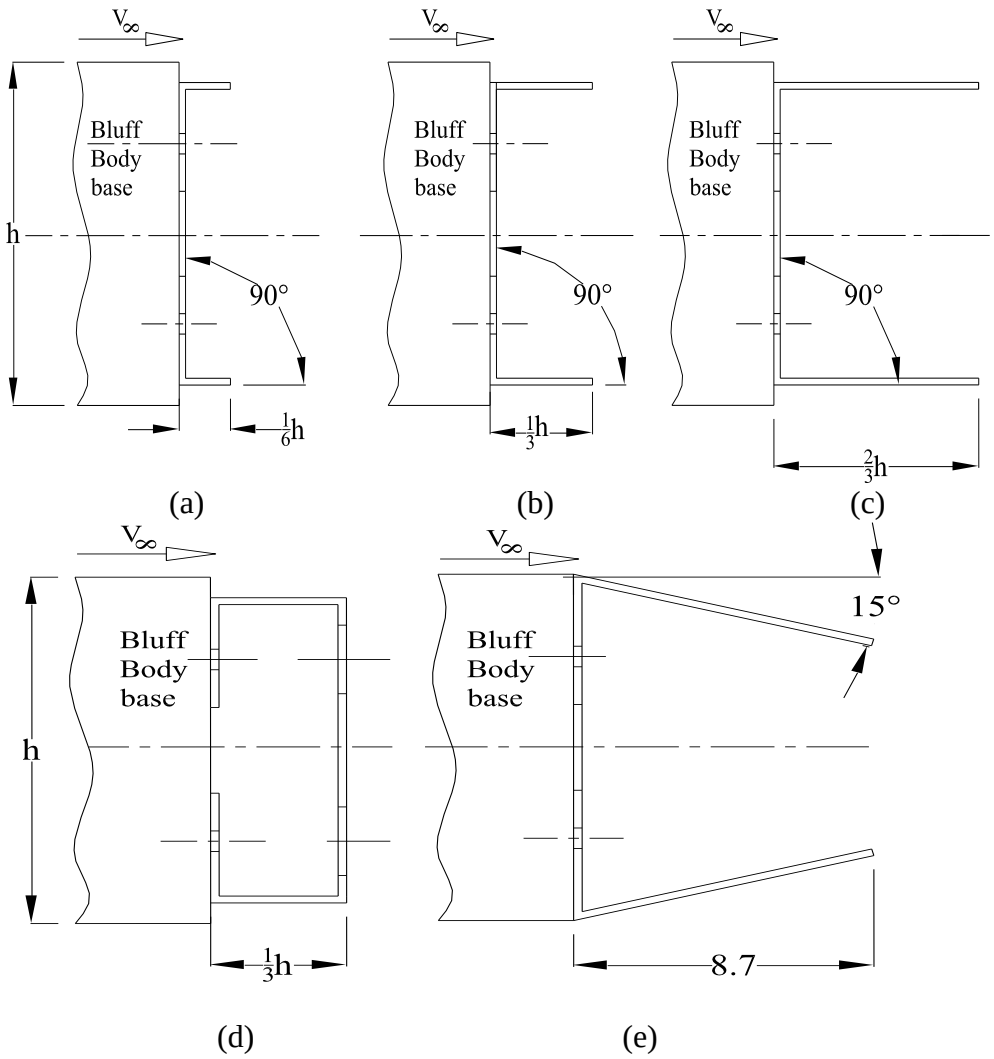

Figure 1.3 Schematic diagram of five cavities used in this investigation, h = 50 mm. Dimensions are in mm.

1.4.1 Objectives

Therefore the objectives of this experimental investigation are:

- To determine the effects of different cavities on the base pressure and drag of a two-dimensional bluff body.

- To determine the effects of the best three drag reducing cavities on the vortex shedding phenomenon.
- To study the wake flow structure behind the best performing cavities using PIV.

In order to achieve the above objectives, the following measurements were conducted.

Steady base pressure measurements:

The steady pressure measurements were obtained at 19 pressure ports installed at the base of the model for the reference geometry as shown in Figure 1.4. For the cavities the pressure ports No. 8, 9, 11, 12 were not accessible, due to the attachment of the cavity with the base model, and therefore the steady pressure is obtained at port Nos. 1-7, 10 and 13-19. The dimensional details of all the pressure ports are shown in table 2.1 in section 2.2.

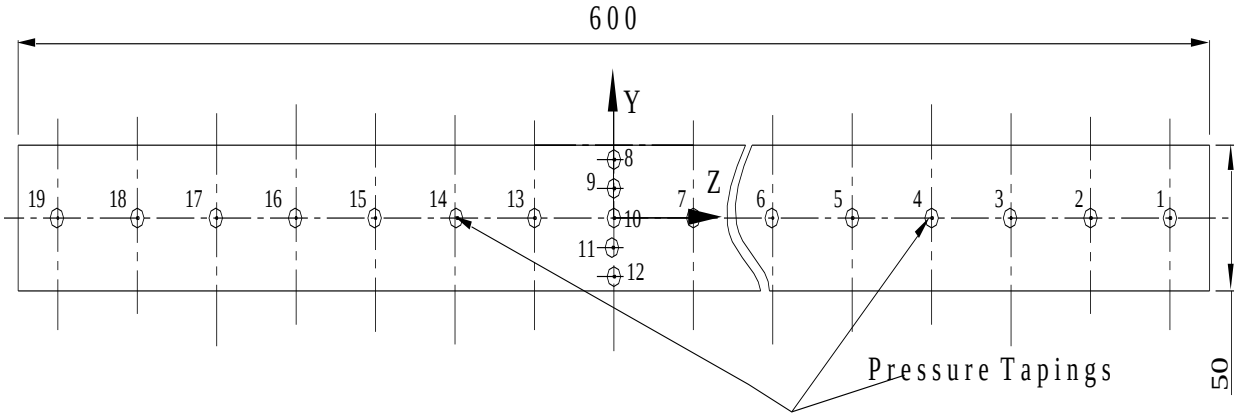

Figure 1.4 Distribution of pressure tapings at the base of the bluff body model. Dimensions are in mm. Figure not to scale.

Drag-Force measurements:

The drag force were determined for the reference geometry and the cavities installed by using the momentum integral method formula :

$$D = \rho b \int U_1 (U_1 - U_2) dy \quad \text{..... (1.1)}$$

where U_1 is the velocity upstream of the model and U_2 is its velocity downstream. This allows us to determine which modification has more drag reduction. As mentioned above, of the five modifications considered in this study, the three best drag reduction modifications will be considered for further investigations.

Unsteady base pressure measurements:

The unsteady pressure will be scanned at Port No. 10 to determine the effect of geometry modifications on the vortex shedding phenomena.

PIV (particle image velocimetry) measurements:

The PIV measurements will be obtained at selected planes in the near wake of the reference geometry, and the three modifications will be chosen on the basis of the drag-force measurements.

CHAPTER 2

EXPERIMENTAL SETUP AND TECHNIQUES

2.1 Wind tunnel details

The experiments were conducted in the low-speed, low-turbulence wind tunnel of the Wind Tunnel Laboratory at the Department of Aerospace Engineering at King Fahd University of Petroleum and Minerals as shown in Figure 2.1. The tunnel test section of 800 x 600 x 2600 mm is closed, horizontal and designed with a Plexiglas window in the top and sides to provide adequate illumination and viewing for non-intrusive visualization study. The contraction ratio of the nozzle is about 6.5 and the return circuit is partially open. The tunnel is powered by a 5.8 kW motor operating a centrifugal fan. The airspeed in the test section can be varied from 1-35 m/s with a turbulence intensity of less than 0.2%.

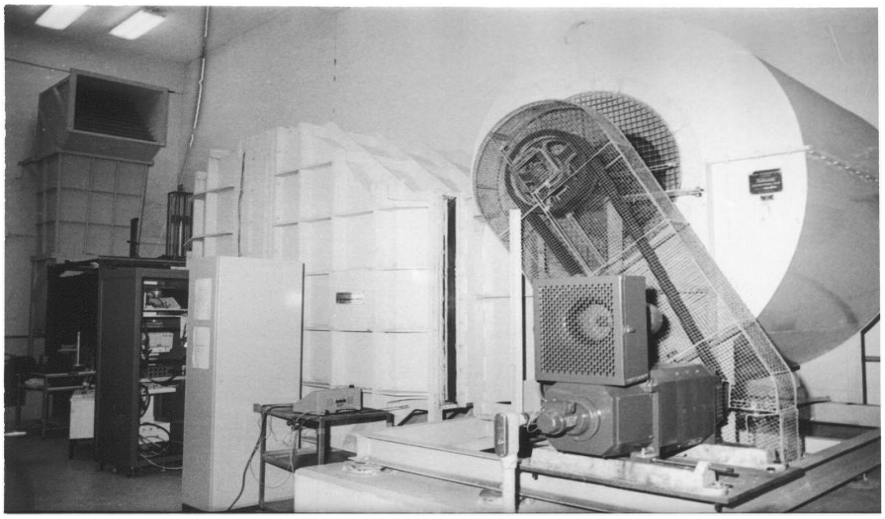

Figure 2.1 Photographic view of wind tunnel.

2.2 Bluff body and cavity details

The bluff body model used has an elliptical leading edge of semi-major axis of 202 mm and a height of 50 mm (8:1 ratio) as used by Bearman [1]. The width of the model is 600 mm as shown in figure 2.2. The blunt trailing edge of this forebody is attached to a metallic frame covered with end plates.

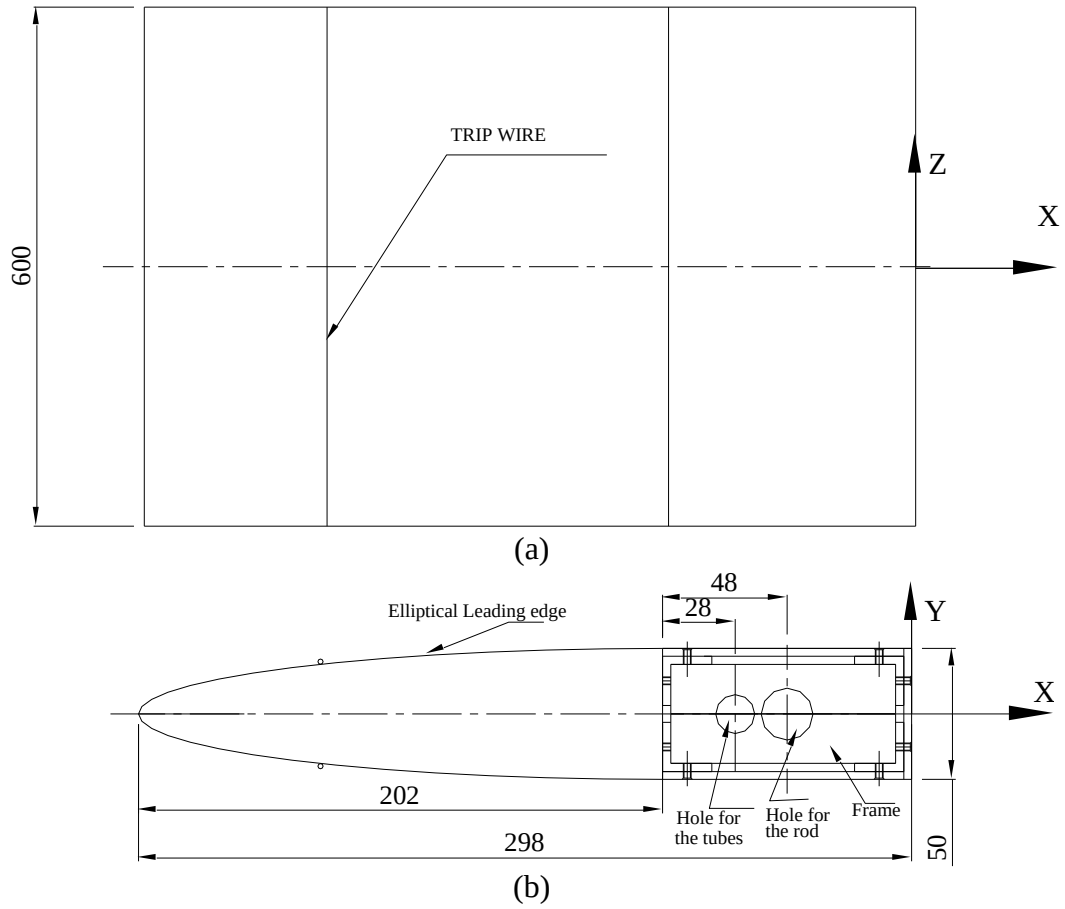

Figure 2.2 Schematic diagram of bluff body model: (a) Top view; (b) Front view. Dimensions are in mm. Figure not to scale.

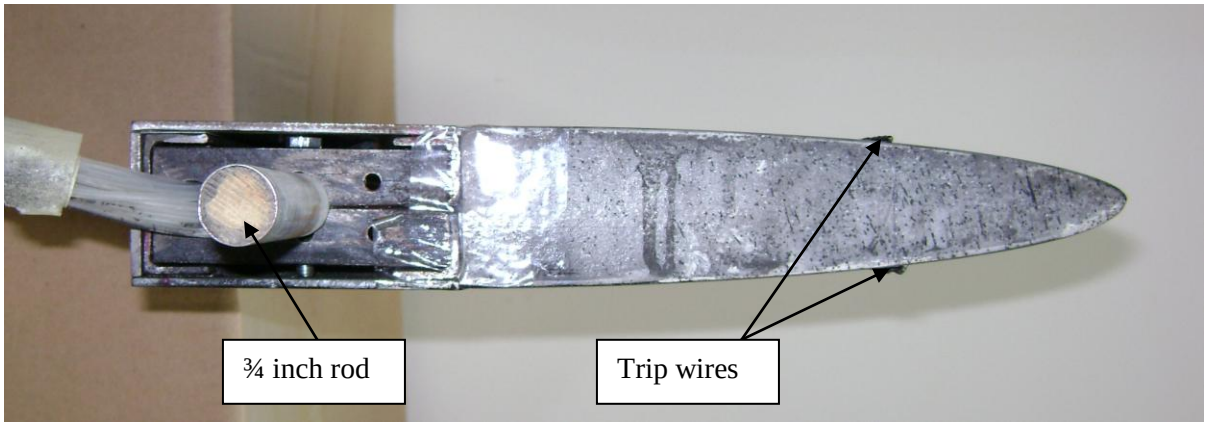

Figure 2.3 Photographic view of bluff body model.

The elliptical part of the bluff body is made out of foam (Styrofoam) cut by a CNC wire-cutting machine. It is then covered with fiber-glass, and sanded well to obtain the desired surface finish to avoid turbulence in flow when it is experimented. The rear part of the bluff body has a welded metal frame made of M.S. (Mild Steel) covered by 2 mm-thick sheet metal made of G.I. (Galvanized Iron). The length of the frame is 96 mm, and its height and width are the same as that of the foam (50 mm and 600 mm, respectively). The front part of the model was then glued to the rear part of the model. The total length of the model is around 298 mm. The model was then black-painted to avoid reflections from laser light during PIV measurements as shown in figure 2.3. The blockage ratio of the model is around 5.0 %. Two holes of diameter 15 mm and 20 mm were made on the side of the model at streamwise locations of 230 mm and 250 mm, respectively. The first was used to direct pressure plastic tubes to the manometer outside the tunnel. A ¾" OD rod goes through the second hole and rests on two posts in both sides of the end plates to support the model as shown in figures 2.4 and 2.5. The base of the model was instrumented with 19 pressure ports.

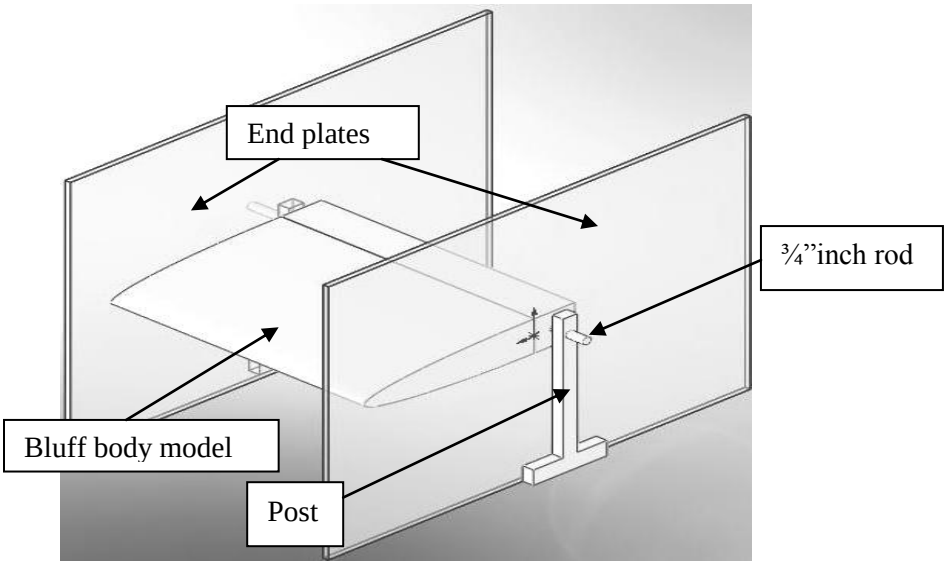

Figure 2.4 Schematic view of the bluff body model mounted in the wind tunnel.

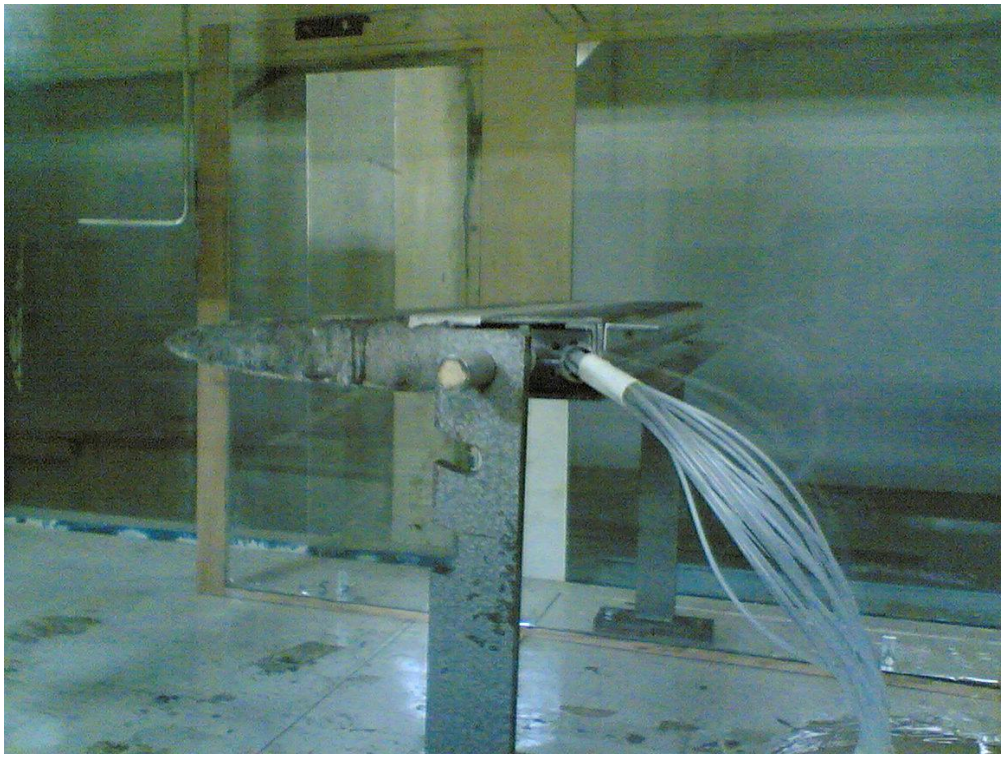

Figure 2.5 Photographic view of bluff body model mounted in the wind tunnel.

Table 2.1 lists the coordinates of 19 pressure ports located on the base of the bluff body model. The location of pressure port 10 is the location where X, Y, Z = 0, (i.e., the origin) as shown in figure 1.4 in section 1.4.1.

Table 2.1 Coordinates of the pressure ports located on the base of the bluff body model.

Pressure Port No.	X (mm)	Y (mm)	Z (mm)	Pressure Port No.	X (mm)	Y (mm)	Z (mm)
1	0	0	280	11	0	-10	0
2	0	0	240	12	0	-20	0
3	0	0	200	13	0	0	-40
4	0	0	160	14	0	0	-80
5	0	0	120	15	0	0	-120
6	0	0	80	16	0	0	-160
7	0	0	40	17	0	0	-200
8	0	20	0	18	0	20	-240
9	0	10	0	19	0	10	-280
10	0	0	0				

Tripping of Base model:

In order to test the model in the turbulent flow regime, and to compare the results of this model with that of the ones in literature, tripping of the model was necessitated. A black

trip wire of length 600 mm and 2mm diameter was placed along the span at a distance of 75 mm from the leading edge of the model on the upper and lower surface of the model.

Details about the cavities:

The cavities are made of 1 mm thick aluminium sheet, bent to the desired shape and size, and holes are drilled accordingly as shown in figures 2.4 to 2.8. All the dimensional details of the cavities are given in the figures below. The dimensions of these cavities were selected on the basis of the work done by Cooper [34] and Lanser [42], who used similar cavities for drag reduction on bluff bodies (e.g. truck and full scale tractor/trailer respectively). For the 3-D truck model (FORD LN700), Cooper [34] attached a three-sided base cavity at the rear end of the bluff body. This cavity was made in the form of thin panels with 15^{o} inclination given to the cavities with respect to each side. The slant cavity length (l) of these panels were obtained by the formula

$$l = \bar{l}\, h \qquad \text{(2.1)}$$

where $\bar{l}$ is a dimensionless number equal to 0.18 and h is the height of the bluff body in mm. Based on this formula, the slant cavity length of angled cavity used in our experiment was calculated and found to be 9 mm as shown in figure 2.6.

These cavities are expected to bring down the drag, and will be experimented and investigated on a two-dimensional bluff body. Also, the effects of these cavities on the near wake flow behind the body will be studied.

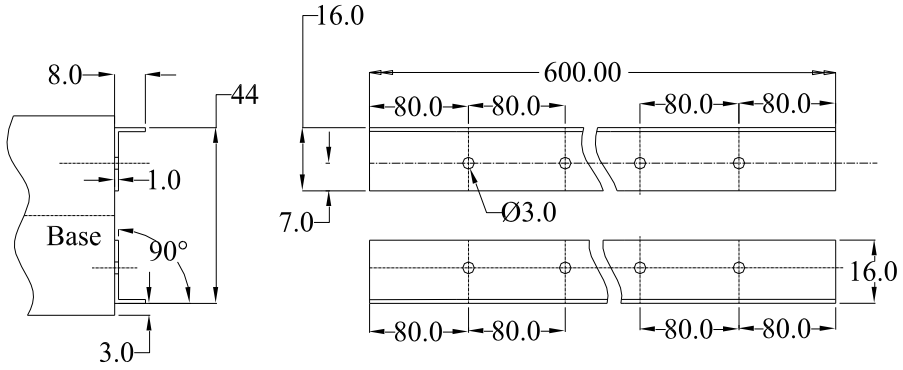

Figure 2.4 Schematic diagram of 1/6 h cavity. Dimensions are in mm. Figure not to scale.

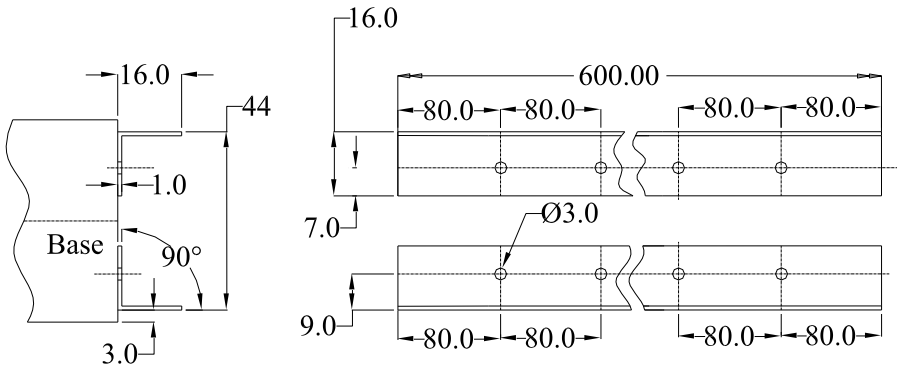

Figure 2.5 Schematic diagram of 1/3 h cavity. Dimensions are in mm. Figure not to scale.

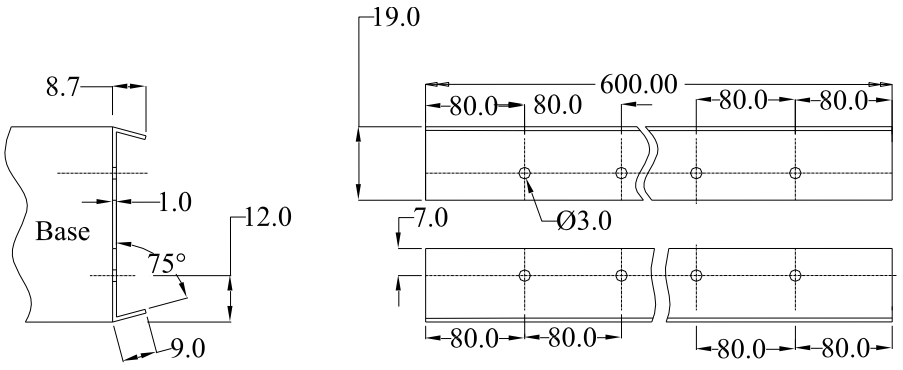

Figure 2.6 Schematic diagram of angled cavity. Dimensions are in mm. Figure not to scale.

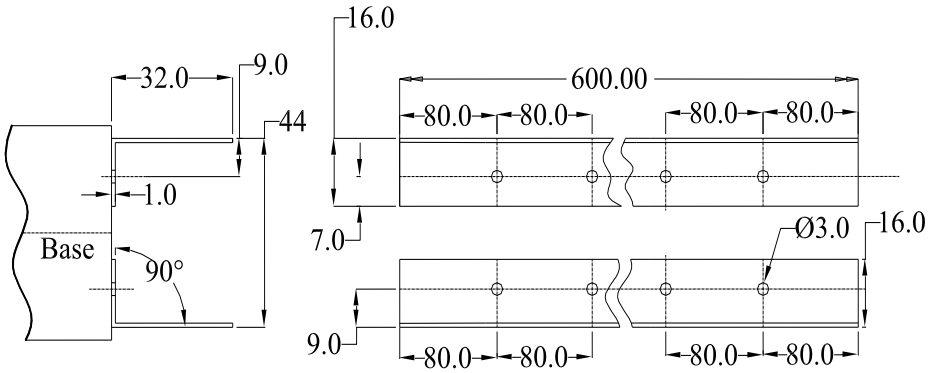

Figure 2.7 Schematic diagram of 2/3 h cavity. Dimensions are in mm. Figure not to scale.

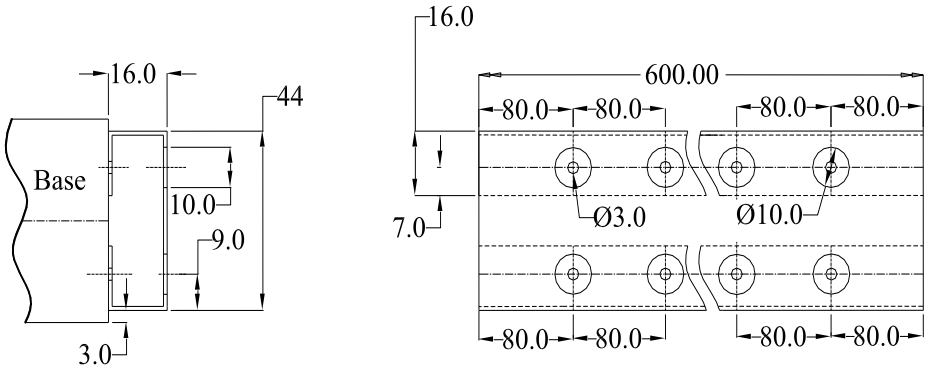

Figure 2.8 Schematic diagram of 1/3h closed C-cavity. Dimensions are in mm. Figure not to scale.

2.3 Pressure Measurements Techniques

2.3.1 Steady base pressure measurements

The steady base pressure and the velocity were measured by using a multi-tube Manometer in which there are 36 tubes to measure 36 pressure points at the same time. The manometer liquid is oil, and its specific gravity is 0.784. The pivoted construction allows the frame of the tubes to be tilted to a maximum of 10^{o} angle inclined from horizontal in order to increase measurement resolution.

The static and dynamic pressures in the wind tunnel were measured by using a pitot tube. The tube was fixed to the roof of the test section, and placed at mid distance between the model and roof of the tunnel to account for the blockage ratio.

To calculate the steady base pressure of the two-dimensional bluff body, 19 pressure ports that were installed at the base of the bluff body model were connected to the manometer by using plastic tubes. The manometer was tilted to a 30^{o} angle to increase measurement resolution. The static and stagnant ports of the Pitot tube were also connected to the manometer to measure the free stream velocity at which the experiment was carried out. A digital camera was placed on a tripod parallel to the plane of the manometer, and about 10 images were captured for the base model and the cavities. The images were then by processed using Adobe Photoshop to obtain the Cp for the base model and the cavities. The flow acceleration due to the presence of the model is considered small (7.35 to 7.94 m/s). The base pressure coefficient is calculated by using the formula

$$C_p = \frac{P - P_\infty}{P_0 - P_\infty} \quad \text{..... (2.2)}$$

where C_p is the base pressure coefficient, P is the pressure measured at the pressure ports of the base model, P_0 is the stagnation pressure, and P_∞ is the reference pressure (static pressure).

2.3.2 Unsteady pressure measurements

The fluctuations of the pressure in the near wake of the bluff body model were measured by using a Scani-valve system. The Pressure Port No. 10 of the base model, located at the center of the base, and the static and stagnant ports of the Pitot tube, were connected to

the pressure transducer. The range of the pressure transducer was ±10 mm of water. The length of the pressure tube to connect the Pressure Port No. 10 with the transducer was around 0.6 m. The data were collected at a sampling frequency of 2000 Hz. The measured pressure values were stored in the form of DAT files in the system. To ensure the repeatability of the measurements, 10 sets of data were acquired over a period of 10 minutes. The data were then processed in MATLAB software using the P-Welch method to determine the spectrum of the pressure coefficient fluctuations and vortex shedding frequency.

The pressure fluctuation spectrum Φ_{pp} (f) is defined as the Fourier transform of the pressure fluctuation autocorrelation $R_{pp}(\tau)$

$$\Phi_{pp}(f) = \int_{-\infty}^{\infty} R_{pp}(\tau) \exp(-i2\pi f\tau)\, d\tau \quad \text{..... (2.3)}$$

$$R_{pp}(f) = \int_{-\infty}^{\infty} \Phi_{pp}(f) \exp(-i2\pi f\tau)\, df \quad \text{..... (2.4)}$$

where f is the frequency in Hz, and τ is the autocorrelation time delay in seconds. The flow is assumed stationary and therefore the pressure fluctuation autocorrelation is given by

$$R_{pp}(\tau) = \lim_{T\to\infty} \frac{1}{T} \int_{0}^{T} p'(t)\, p'(t+\tau) dt \quad \text{..... (2.5)}$$

where $p' = p - \overline{p}$ is the pressure fluctuations.

The non-dimensional form of pressure fluctuations is the pressure coefficient fluctuations, $c'_p = p'/q$, where q is the dynamic pressure; the non-dimensional form of the

pressure fluctuation autocorrelation is $\overline{R_{pp}} = R_{pp}/q^2$; and the non-dimensional spectrum is $\overline{\Phi_{pp}} = \Phi_{pp}/q^2.U/h.$

2.4 Drag-Force Measurements Techniques

A two-dimensional traverse mechanism was used to scan the velocity profiles along the vertical direction (normal to the free stream) upstream and downstream of the bluff body model. The traverse mechanism is driven by a stepper motor. It moves in steps, and each step is 0.025 mm. It can move in vertical and horizontal directions. The pitot-tube was attached to the traverse mechanism by using an aluminium rod.

The drag force, *D*, acting on the body is determined by using the Momentum Integral formula

$$D = \rho b \int U_1(U_1 - U_2)\,dy \quad \ldots\ldots\ldots\ldots\ldots\ldots\ldots\ldots\ldots\ldots \quad (2.2)$$

where ρ is the air density, U_1 is the velocity upstream of the model, U_2 is the velocity downstream side of model and *b* is the width of the model. The velocity upstream of the model (U_1) was scanned at 30 points along the vertical direction at a position located 120 mm upstream of the model. Similarly the velocity downstream of the model, U_2, was scanned at 30 points along the vertical direction at a position located 250 mm downstream of the model.

2.5 PIV Measurements Techniques

The PIV (Particle Image Velocimetry) measurements are used to visualize the flow and obtain velocity fields in the near wake of the bluff body. The flow was illuminated by

using two Nd-YAG lasers (New Wave 120). Both the lasers can be operated at approximately 120 mJ per pulse (operated around 100 mJ per pulse in this experiment). The output laser beams were merged and directed into the test section by a set of mirrors. The resulting beams were shaped into a light sheet by a combination of a 1000 mm focal-length spherical lens and a 6.35 mm focal length cylindrical lens. This optical setup which is shown in Figure 5.1, produced a laser sheet 0.5mm thick by 500mm at the measurement location i.e. at the midspan (Z = 0). The whole optical setup was mounted on an external rig fixed to the floor of the lab to minimize vibrations. The lasers were synchronised to illuminate the flow twice with a short time delay between the two exposures (~60 μs). A high-resolution dual-frame digital camera (1600 x 1200 pixels), mounted on a tripod outside the tunnel, was used to record the PIV images.

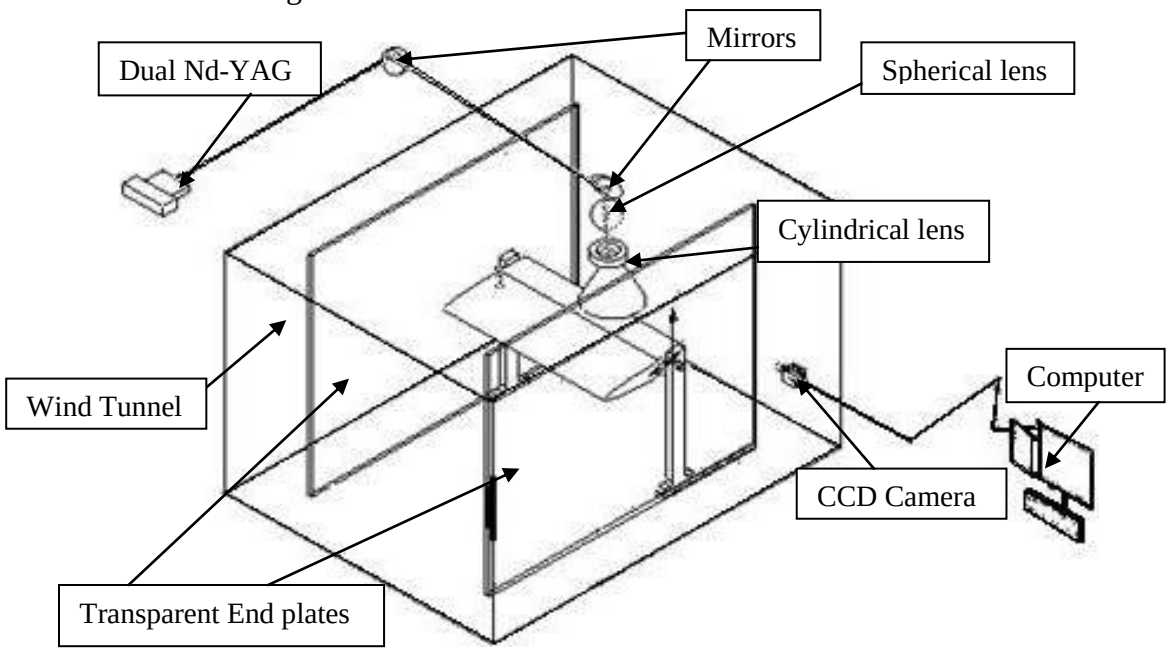

Figure 2.9 Schematic diagram of the PIV setup for the Bluff body model mounted in the wind tunnel.

The flow was seeded with small oil droplets generated by an oil pump equipped with an atomizer. The oil is injected upstream of the settling chamber at midspan. The target particle displacement was selected to minimise noise. If the target displacement is too small the uncertainty in the particle displacement measurement increases. If the target displacement is too large, a large number of particles may leave or enter the light sheet between exposures degrading the performance of the peak detection algorithm used in the particle displacement measurement. The target displacement measurement was 4 pixels. A total of 300 images were recorded at each test condition. The laser, camera and shutter were synchronized by using a delay generator triggered by using DAVIS software.

The PIV images were processed by using an image shifting algorithm consisting of two steps. In the first step, the images were processed by using a standard cross correlation algorithm with un-shifted interrogation windows to determine the particle displacement at each grid point. The interrogation window size is large enough to accommodate the expected particle displacement. In the second step, cross correlation analysis between shifted interrogation windows was used. The window shift at each grid point is the particle displacement obtained in the first step. The advantage of this technique is that the noise level is reduced. The interrogation window used in the second step determined the spatial resolution of the measurement. In all cases, the interrogation window used was 64 x 64 pixels and the grid spacing was 16 pixels. The image resolution was 11.3 pixels/mm. The PIV data obtained were processed by using MATLAB to get the mean properties at each test condition.

CHAPTER 3

BASE PRESSURE AND DRAG-FORCE MEASUREMENT RESULTS

3.1 Steady Base-pressure measurements

3.1.1 Base model

The Steady and Unsteady pressure, drag-force and PIV measurements were taken at a free stream of ~ 8m/s corresponding to a Reynolds number of 2.6×10^4 based on the height of the model. Before testing the various cavities considered in this study to determine their effects on the base pressure and the drag of the body, it was important to measure the base pressure and drag of the base model. The base pressure and drag values of the base model served two purposes:

- They were used as reference values in order to calculate the change made by the cavities.
- The obtained values of the base model agreed with the previous results found in the literature (by Bearman [1] and Park [8]) and thereby assured us that our experimental methodology was correct.

The trip wire was located at a distance of about 20% from the leading edge. This location was chosen based on the previous works done by Bearman [1], Park [8] and other researchers in which they tripped the leading edge of the bluff body model at around 20%.

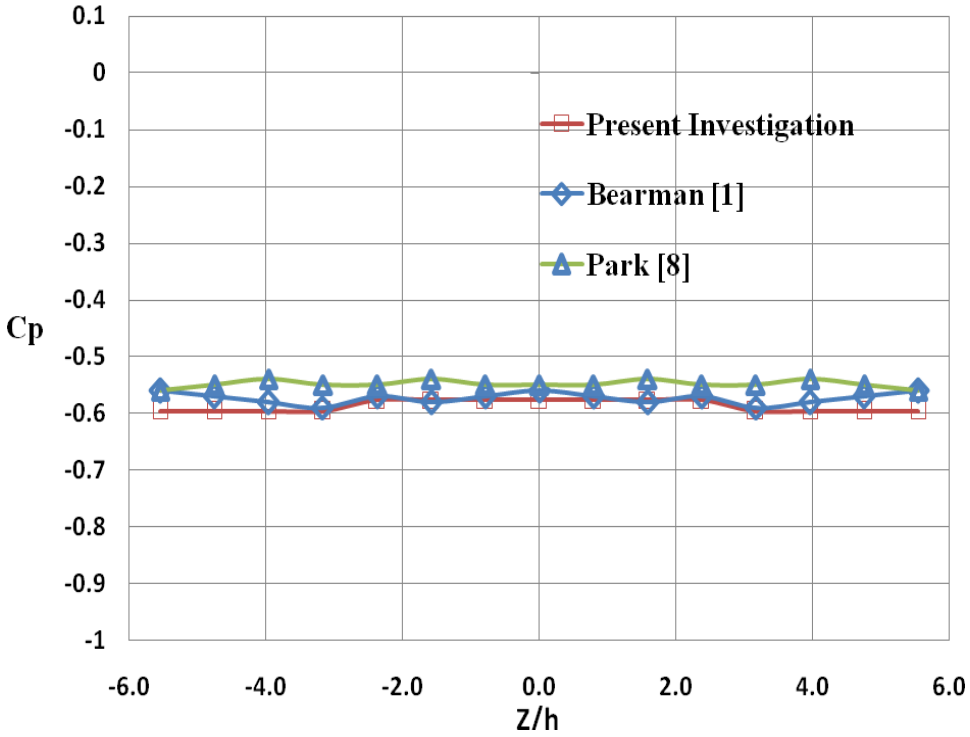

Figure 3.1 Base pressure distribution across spanwise direction for the base model.

Figure 3.1 shows the base pressure distribution along the spanwise direction for the base model. As can be seen, the pressure coefficient is almost constant along the span except near the wind tunnel walls, where the pressure is lower. The Cp obtained ranges from -0.6 near the wind tunnel walls to -0.58 at midspan. As can be seen, the pressure distribution obtained in this study agrees with Bearman [1] and Park [8].

3.1.2 Base model fitted with 1/6 h cavity

Figure 3.2 shows spanwise pressure distribution at the base of the model fitted with 1/6 h cavity. It is clear from this figure that this cavity increases the base pressure by around 10% compared to base model. Similar to the base model, the pressure coefficient near the

wind tunnel side walls is lower than that around the midspan of the model. The Cp obtained ranges from -0.52 to -0.54 across the spanwise direction.

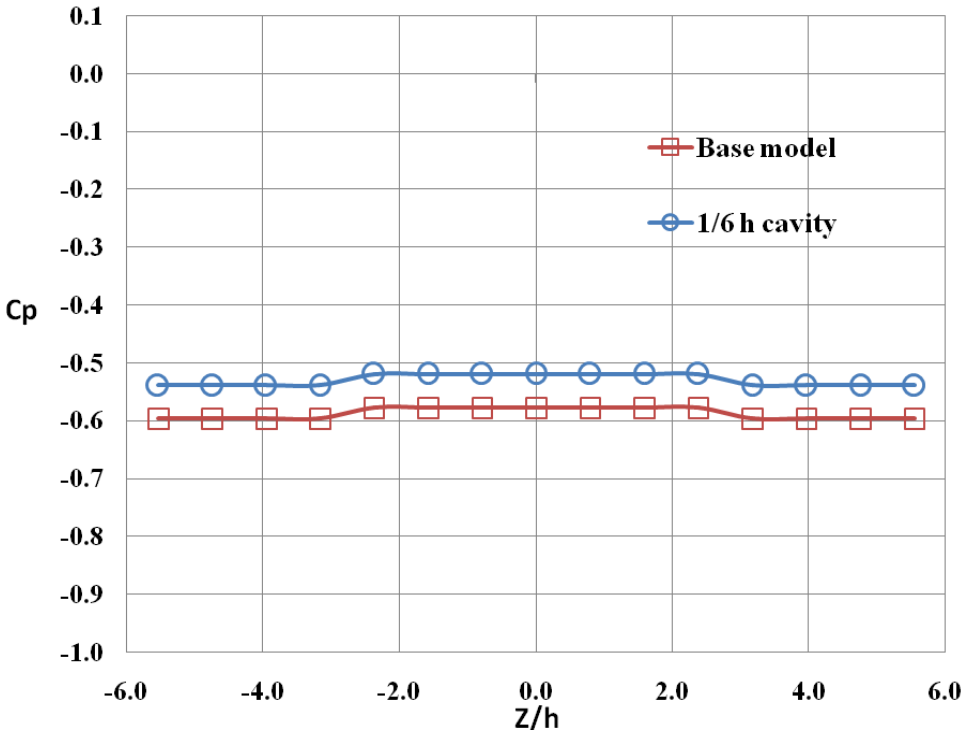

Figure 3.2 Base pressure distribution across spanwise direction for 1/6 h cavity.

3.1.3 Base model fitted with 1/3 h cavity

Figure 3.3 shows the spanwise pressure distribution at the base of the model fitted with 1/3 h cavity. From this figure it is inferred that the base pressure is increased by around 46% (ranging from -0.33 to -0.31), compared to the base model and 36% compared to the 1/6 h cavity.

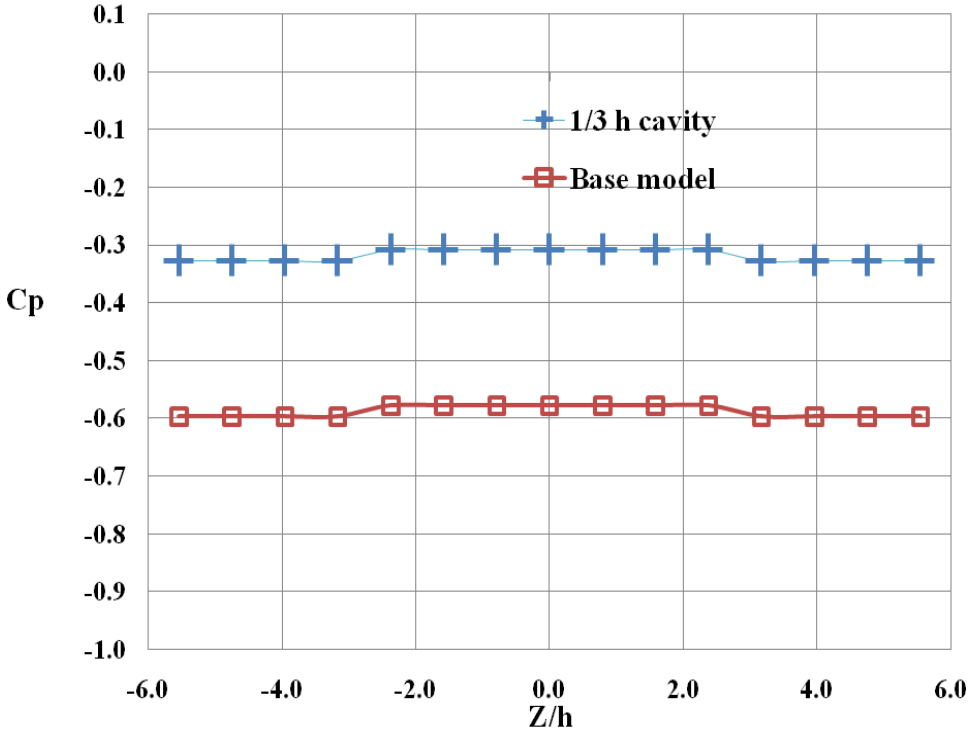

Figure 3.3 Base pressure distribution across spanwise direction for 1/3 h cavity.

3.1.4 Base model fitted with 2/3 h cavity

The spanwise pressure distribution at the base of the model fitted with 2/3 h cavity is shown in Figure 3.4. It is seen from this figure that the base pressure is increased by around 26.5% when the 2/3 h cavity was attached to the base model. This increase in base pressure is higher than the increase due to the 1/6 h cavity by around 16.5% but lower than the 1/3 h cavity by around 20%. The C_p obtained ranged from -0.44 to -0.42 across the spanwise direction.

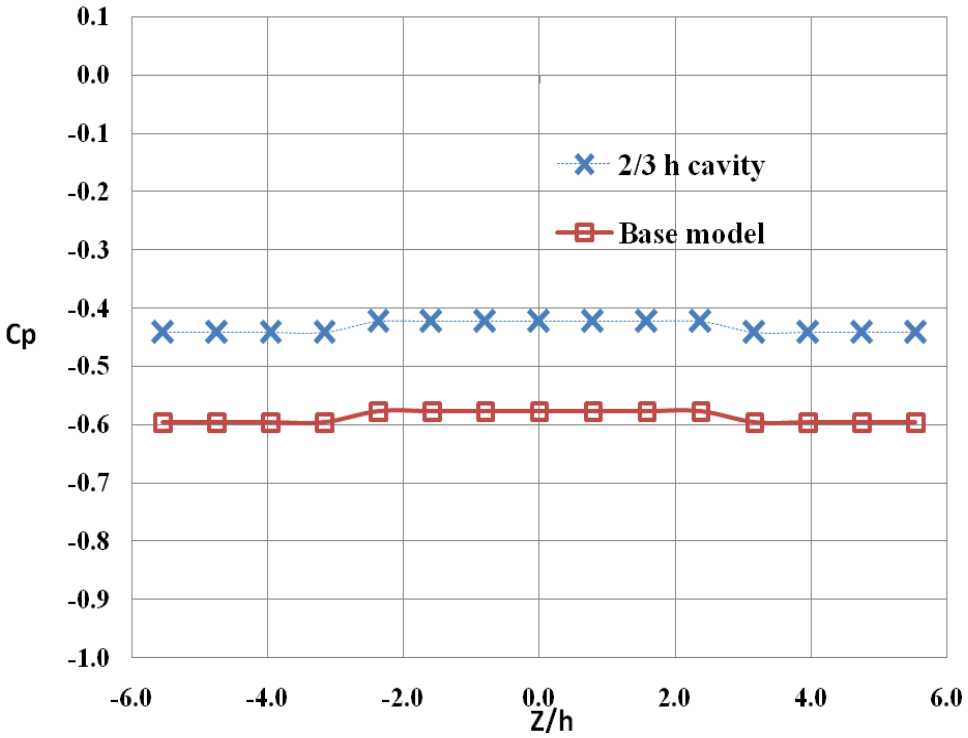

Figure 3.4 Base pressure distribution across spanwise direction for 2/3 h cavity.

3.1.5 Base model fitted with angled cavity

Figure 3.5 shows the spanwise pressure distribution at the base of the model fitted with angled cavity. From this figure it is evident that angled cavity increases the base pressure by around 20%. Similar to the base model and 1/6 h, 1/3 h and 2/3 h cavities, the pressure coefficient near the wind tunnel side walls is lower than that around the midspan of the model. The Cp obtained ranged from -0.48 to -0.46 across the spanwise direction.

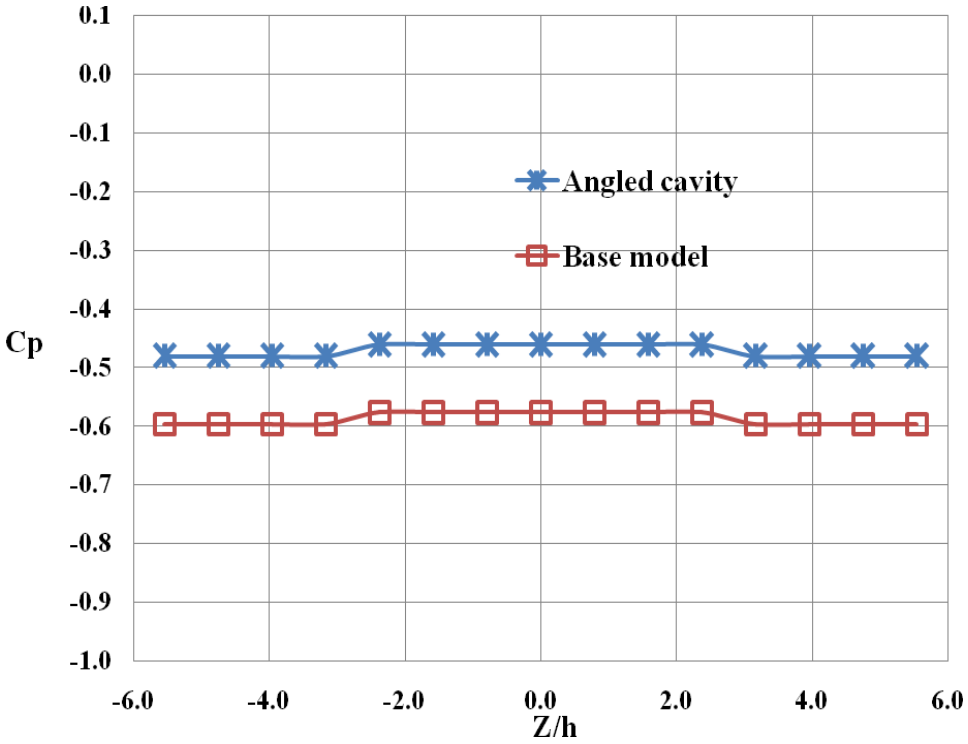

Figure 3.5 Base pressure distribution across spanwise direction for angled cavity.

From the above measurement results, it can be concluded that 1/6 h cavity gives the lowest base pressure rise, and other cavities give a good base pressure rise, which is directly proportional to drag reduction phenomenon for 2-D body, which will be discussed under force measurements in next chapter. The pressure coefficients at the center of the base (pressure port 10) for the base model and the cavities are tabulated in Table 3.1.

Table 3.1 Steady base pressure coefficients at pressure port 10 for the base model and the cavities.

Model	C_p at Pressure port 10
Base model	-0.58
1/6 h Cavity	-0.52
1/3 h cavity	-0.31
2/3h Cavity	-0.42
Angled Cavity	-0.46

3.2 Unsteady pressure measurements

The unsteady pressure measurements were taken at the center of the base (Pressure port No.10) for the base model, 1/3 h cavity, 2/3 h cavity and angled cavity. The measurements were conducted at a freestream speed of 8 m/s corresponding to a Reynolds number of 2.6×10^4 based on the height of the body. Spectra of the pressure fluctuations were obtained by using the P-Welch method.

3.2.1 Base model

Figure 3.6 shows a spectral-frequency plot of the power spectral density versus the frequency for the base model. The figure shows a dominating peak at a frequency of 11 Hz corresponding to a Strouhal number of around 0.07 based on the height of the body. There are some other peaks, but these peaks have lower energy than that located at f ~ 11 Hz.

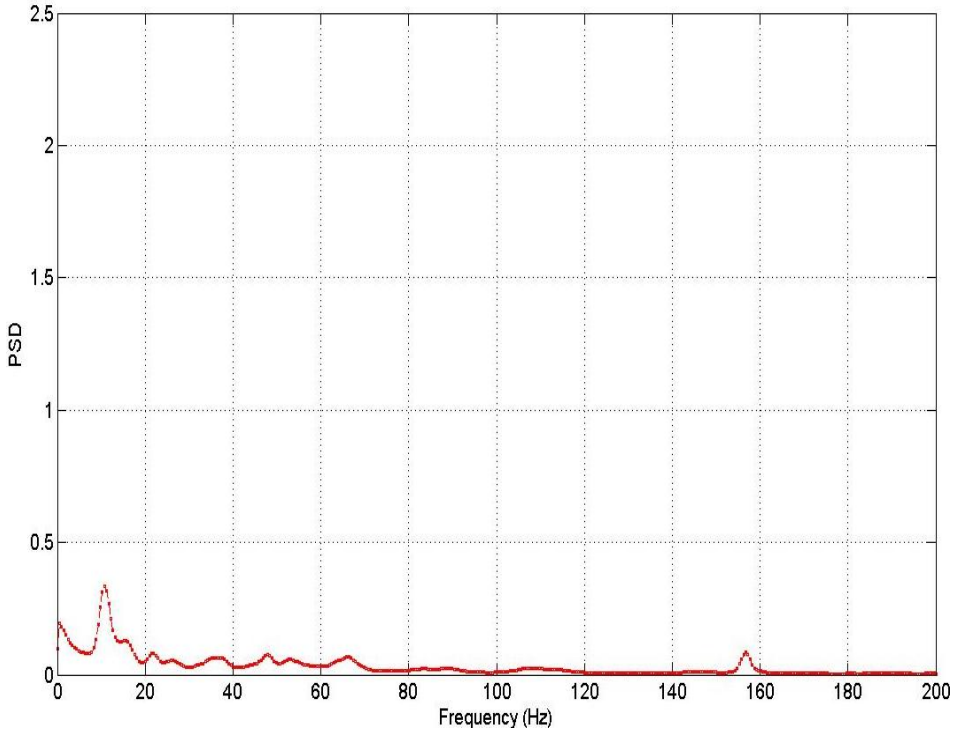

Figure 3.6 Plot of the power spectral density versus frequency measured at pressure port 10 of the base model.

3.2.2 Base model fitted with 1/3 h cavity

Figure 3.7 shows the spectral-frequency plot of the power spectral density versus the frequency of vortex shedding for the base model fitted with 1/3 h cavity. As can be seen from this figure, a dominating peak of the spectrum occurs at the same frequency as the base model (~11 Hz) which corresponds to a Strouhal number of ~ 0.07. This means that the frequency of the vortex shedding has not changed with the attachment of the 1/3 h cavity to the base model. However, this peak has higher energy than the peak of the base model, which means that pressure fluctuations for this cavity are higher than those for the reference model.

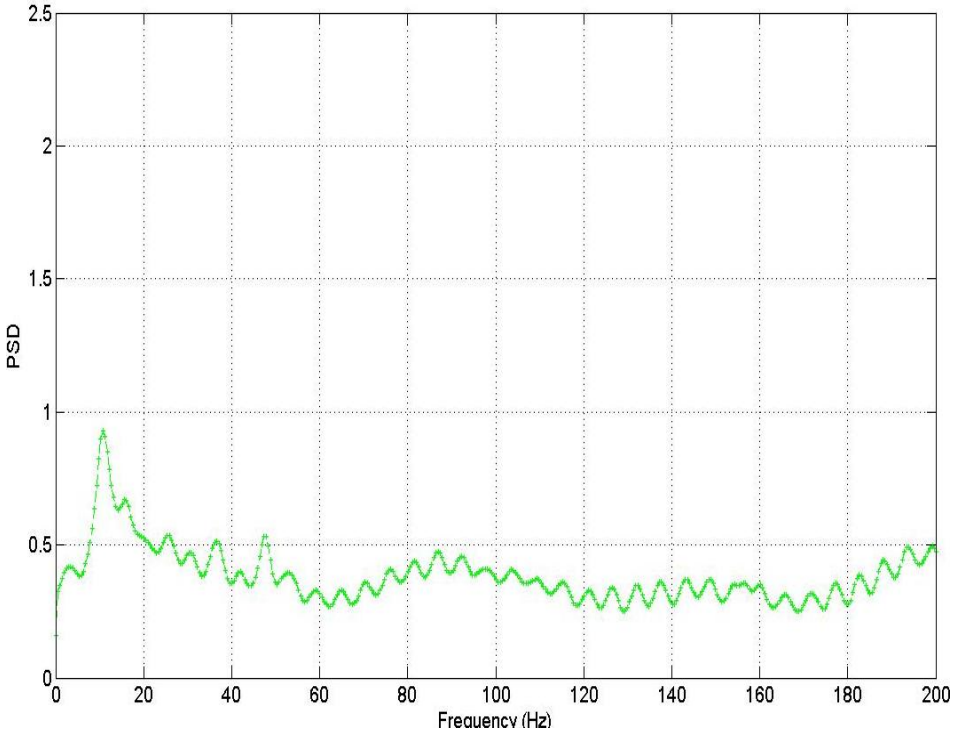

Figure 3.7 Plot of the power spectral density versus frequency measured at pressure port 10 of the base model fitted with 1/3 h cavity.

3.2.3 Base model fitted with 2/3 h cavity

Figure 3.8 shows the spectral-frequency plot of the power spectral density versus the frequency for the base model fitted with 2/3 h cavity. Again this figure shows a dominating peak at a frequency of 11 Hz corresponding to a Strouhal number of ~ 0.07. But the dominating peak in this figure has more energy than the peak obtained for 1/3 h cavity and base model which indicates stronger pressure fluctuations in the near wake of the cavity.

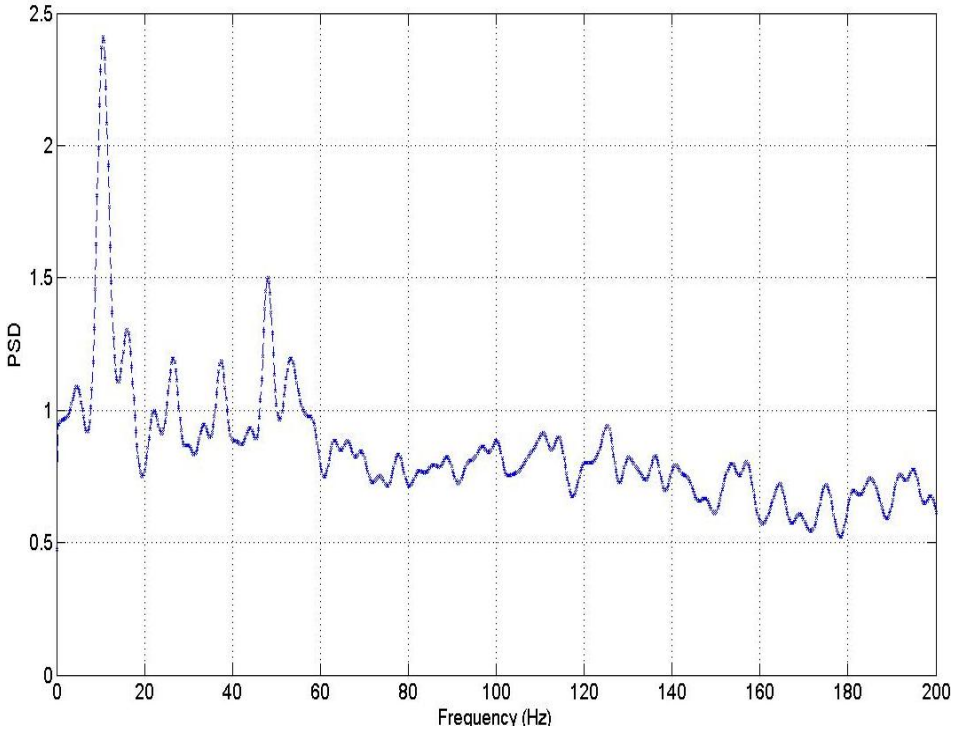

Figure 3.8 Plot of the power spectral density versus frequency measured at pressure port 10 of the base model fitted with 2/3 h cavity.

3.2.4 Base model fitted with angled cavity

Figure 3.9 shows the spectral-frequency plot of the angled cavity. This figure also shows a dominating peak at the same frequency as the other cavities (St = ~ 0.07). The dominating peak in this figure has more energy than base model and 1/3 h cavity but lower than that of 2/3 h cavity peak.

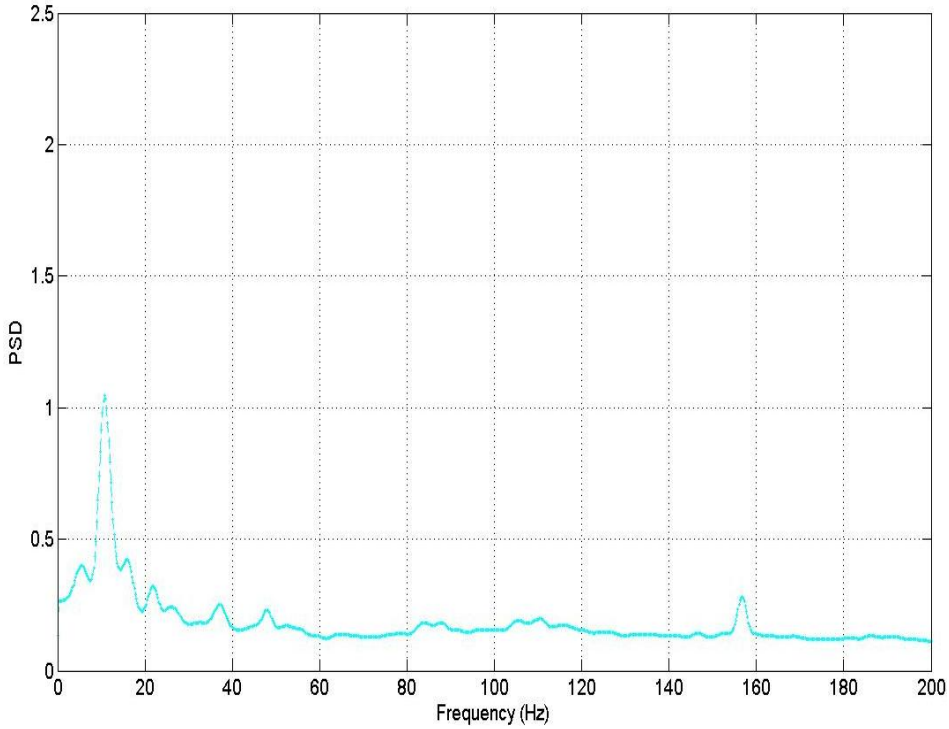

Figure 3.9 Plot of the power spectral density versus frequency measured at pressure port 10 of the base model fitted with angled cavity.

From figures 3.6 to 3.9, it is observed that the dominating peak occurs at the same frequency (~ 11 Hz equivalent to St ~ 0.07) for the base model and for 1/3 h, 2/3 h and angled cavities. This indicates that these cavities have no effect on the frequency of vortex shedding. However, the energy of the pressure fluctuations increased with the attachment of these cavities, which signifies that pressure fluctuations increased with the attachment of the cavities to the base model. This agrees well with the work of Lanser [42] and Morel [3]. This Strouhal number (St ~ 0.07) found in this study is in agreement with the Strouhal number obtained for 3-D bluff body by Duel and George [44] and Al-Garni et al. [46] and comparable to that found by Wu and Faeth [47] for a sphere (St ~ 0.1). The study of Duel

and George [44] is considered to be a thorough study of the vortex shedding phenomena behind a 3-D bluff body. They measured velocity fluctuations at different streamwise locations in the shear layer as well as base pressure fluctuations. The spectra of the velocity fluctuations showed a dominating peak at a Strouhal number of ~ 1. They associated this Strouhal number with vortex roll-up and merging processes in the shear layer. The spectra of the base pressure, however, show a peak at a Strouhal number of ~ 0.07 which is associated with a wake pumping. This wake pumping is the results of the periodic interaction of the upper and lower parts of the trapped vortex in the near wake which causes the free stagnation point to move longitudinally back and forth in a pumping manner.

3.3 Drag-Force measurements

The drag force measurements were taken to obtain the drag reduction of the bluff body and other cavities. The co-efficient of the drag force of the model calculated is given by

$$C_d = \frac{D}{0.5\,\rho U^2\, h\, b} \quad \text{..... (4.1)}$$

where *h* is the height of the model (50 mm) and *b* is the spanwise length (600 mm).

Table 3.2 shows the drag coefficients of the base model and cavities tested. Also shown in the table are the percentage reduction made by each cavity.

Table 3.2 Drag coefficient values of the cavities attached to the base of the bluff body model.

Model	C_d	Percentage reduction in the drag w.r.t the base model (%)
Base model	0.58	----
Base model with 1/6 h cavity	0.52	10.2
Base model with 1/3 h cavity	0.35	38.8
Base model with 2/3 h cavity	0.43	25.1
Base model with angled cavity	0.48	17.1
Base model with closed C-cavity	0.54	6.5

From the table 3.2, it is inferred that the 1/6 h cavity and closed C-cavity gave the least drag reduction (6.5% for closed C-cavity and 10.2% for 1/6 h cavity), compared to the

other three cavities. The 1/3 h cavity has the highest drag reduction which is around 39% followed by the 2/3 h cavity (around 25%) and the angled cavity (around 17.1%).

Figure 3.10 shows the variation of drag coefficient with cavity length for open cavities. From the figure, it can be seen that the C_d value decreases as the cavity length increases, up to 1/3 h (16 mm), but increases when the cavity length is increased to 2/3 h (32 mm).

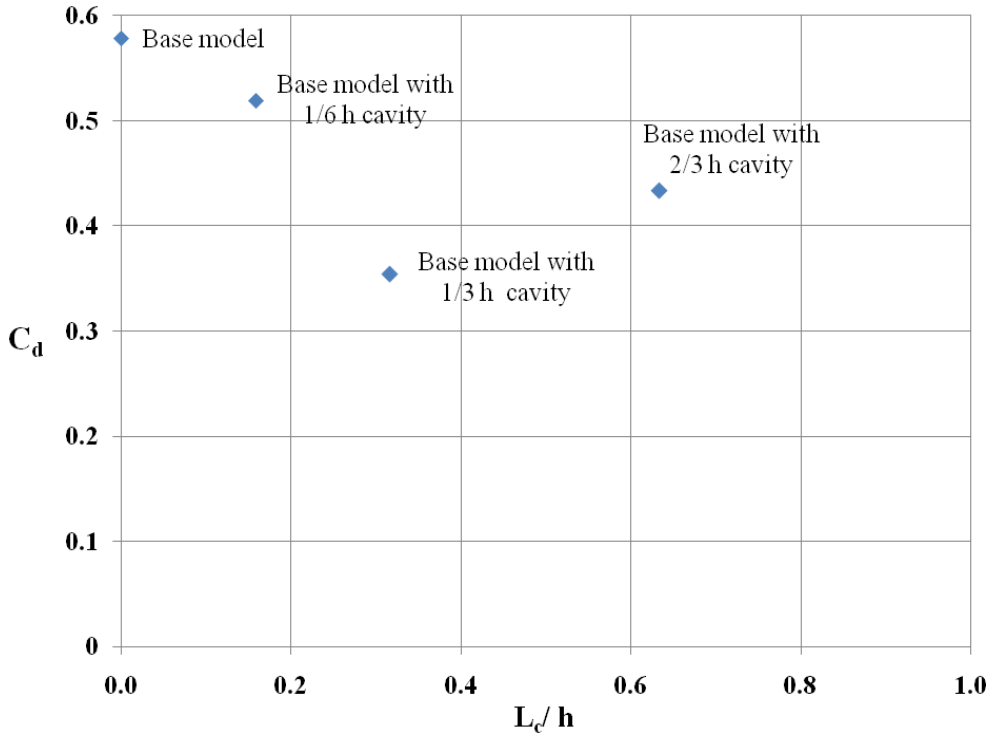

Figure 3.10 Plot of the coefficient of drag (C_d) versus length of the cavity (L_c).

For the 3-D generic automotive bluff body tested by Khalighi et al. [31], the drag coefficient of the base model was found to be 0.3 and with the addition of ½ h open cavity

the drag was reduced by 20%. For the 2-D elliptical bluff body tested by Park et al. [8], 33% decrease in the base drag was observed for the optimal tab configuration.

CHAPTER 4

PARTICLE IMAGE VELOCIMETRY (PIV) MEASUREMENT RESULTS

The PIV measurements were taken in the vertical plane at midspan (Z = 0) for the base model, 1/3 h cavity, 2/3 h cavity and the angled cavity. For each combination of base model and cavities, the PIV set up was calibrated for optimum camera resolution, aperture and focus and focus etc., to obtain the desired image resolution.

4.1 Near Wake Flow

4.1.1 Base model

A typical instantaneous flow field in the vertical plane is shown in figure 4.1. The figure shows normal vorticity contours superposed on the instantaneous velocity vector field. As expected, the shear layer originates at the upper and lower edges of the base model. The shear layer originating from the upper edge is denoted by dotted lines indicating a negative rotation, while the shear layer originating from the lower side is represented by solid lines since rotation is about the positive Z direction. A reverse flow region that gets developed behind the model is observed. There is a sharp, rapid, upward deflection of the underbody flow (i.e. the flow that originates from the lower edge of the base model) at a distance of about 52 mm downstream of the base model. It joins with the flow which comes from the upper edge of the bluff body. Vortical structures are observed farther downstream

of the flow. Although this flow is approximately two-dimensional, the figure shows that this flow is complex and highly unsteady.

Figure 4.2 shows the vector plot of mean velocity field, on which the mean vorticity contours are superposed. The mean velocity flow field plots helps to derive conclusions about the recirculation region and also about the strong reverse flow region that develops behind the bluff body. At the centre of the wake line (Y = 0) the vector lines does not exhibit any upsweep or downsweep in the reverse flow region. It is found that the more the curvature of the flow the more the pressure drop across the shear layers i.e. if the shear layer curves more rapidly towards the centre of the wake, then there is larger pressure drop across the shear layer.

Figure 4.3 shows streamlines of the mean flow field behind the base model. The length of the recirculation region (x_R) is around 48 mm i.e. almost equivalent to base model height (the length of the recirculation region is defined as the distance from the edge of the model to the point where, streamwise velocity u_m reaches zero). There are two circulatory regions, with directions of rotation opposite to each other. The figure shows that recirculation regions formed in the near wake of the model are symmetric with respect to the center wake line (Y = 0). In the reverse flow region the maximum upstream velocity (i.e. the flow in the reverse direction) is approximately 26 % of the free stream velocity.

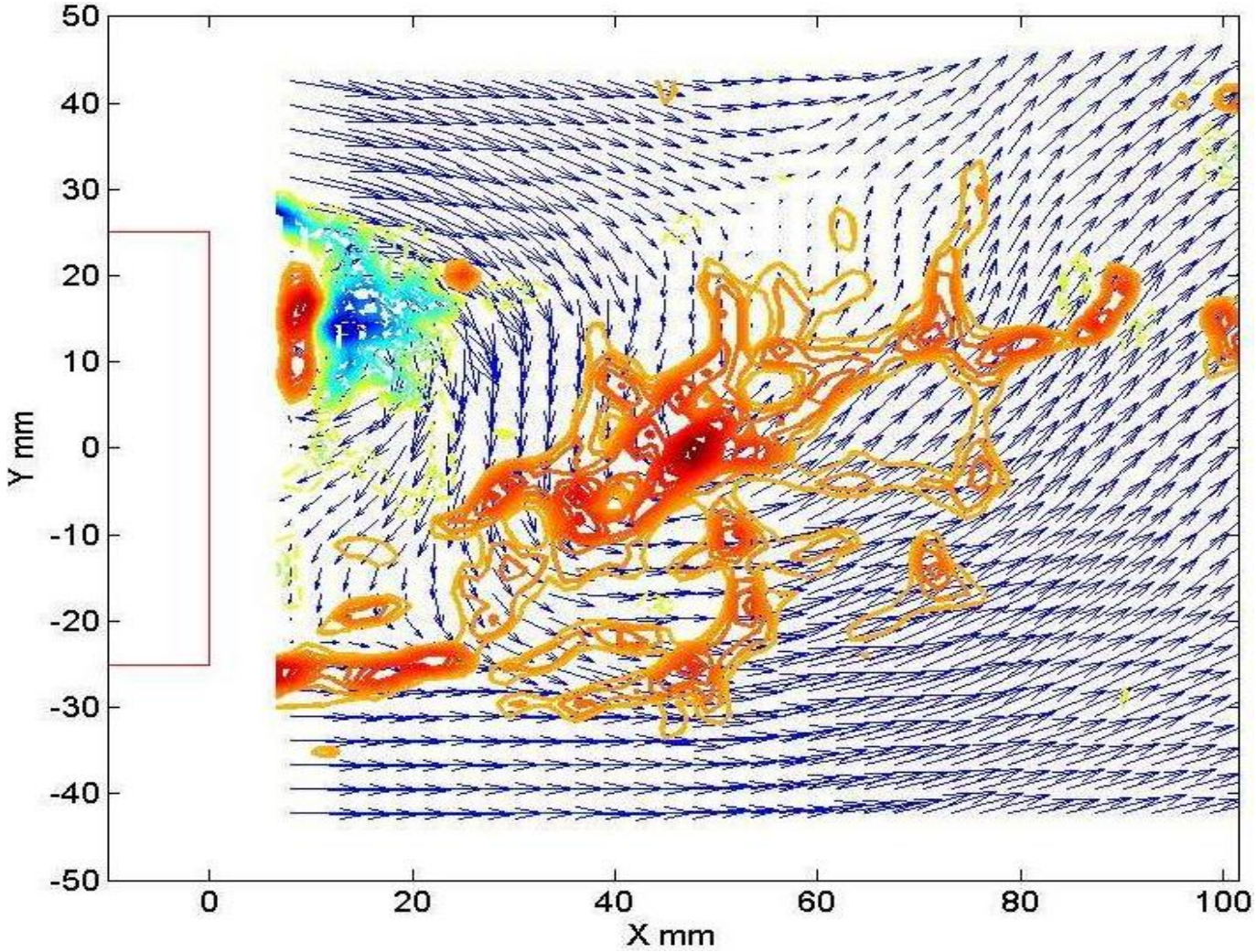

Figure 4.1 Instantaneous velocity and vorticity fields in the symmetry plane of the base model.

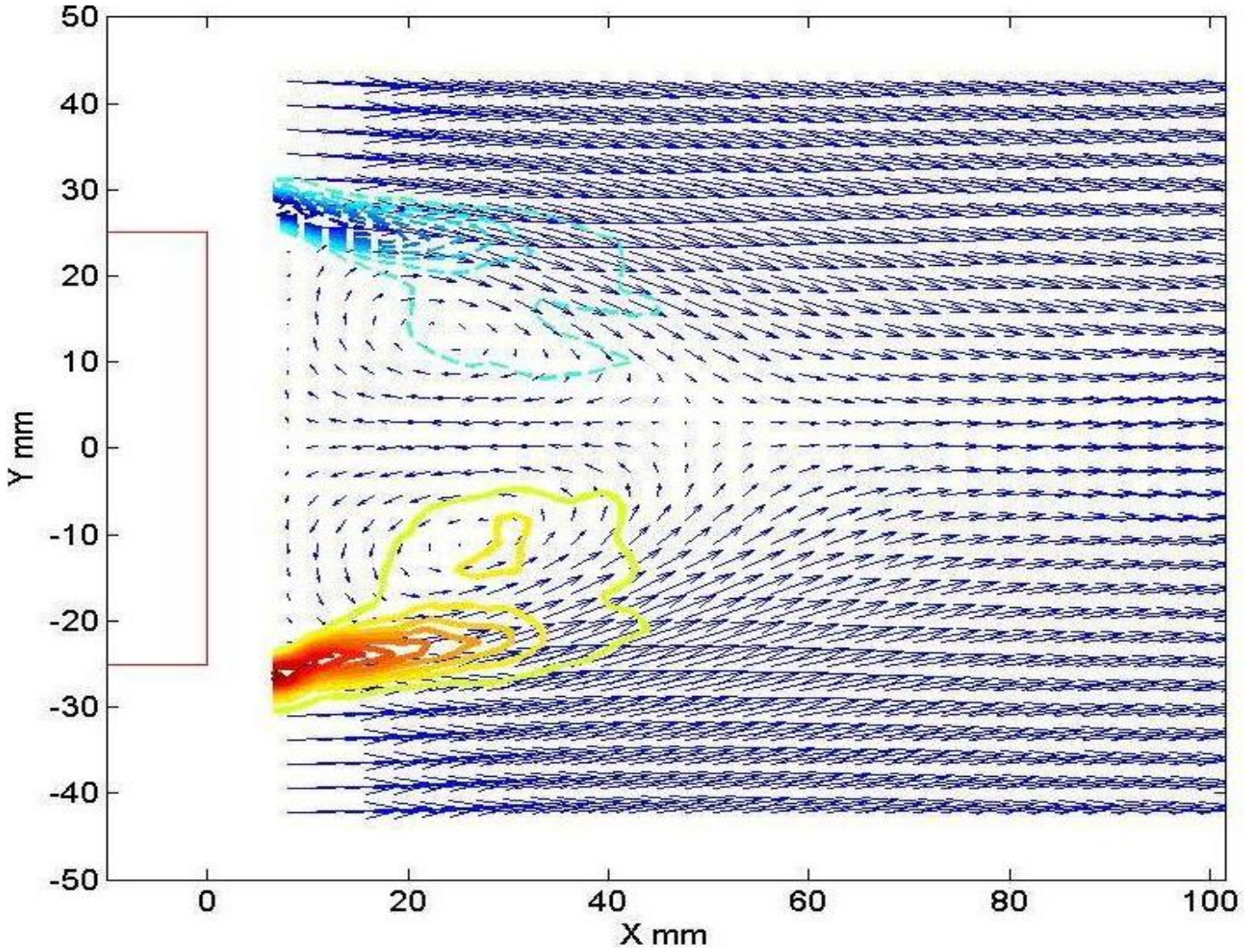

Figure 4.2 Mean velocity and vorticity fields in the symmetry plane of the base model.

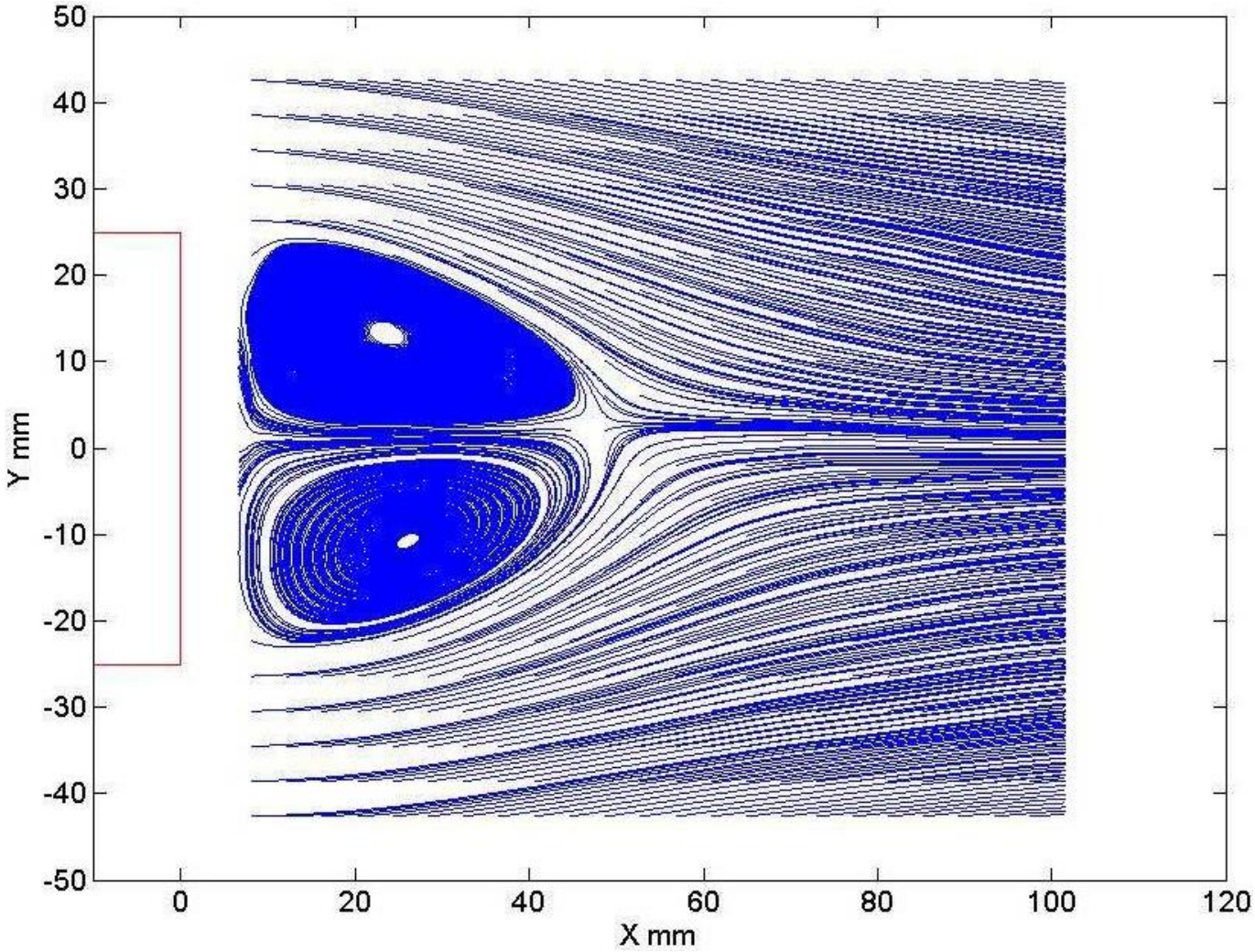

Figure 4.3 Streamlines of the mean velocity field in the symmetry plane of the base model.

4.1.2 Base model fitted with 1/3 h cavity

The PIV measurements were also conducted for the bluff body fitted with the 1/3 h cavity. A typical instantaneous flow field which is measured in the vertical plane (Z = 0) of the base model fitted with the 1/3 h cavity, is shown in Figure 4.4. The vorticity contours are superposed on the instantaneous velocity vector. It was not possible to obtain velocity field data in the near wake of the body between the cavity walls, due to inadequate laser illumination caused by the presence of upper cavity wall. As shown in Figure 4.4 the shear layers originate from the upper and lower edges of the cavity. The two shear layers extend to a larger distance (approximately 80 to 82 mm) in the downstream flow field. Again this figure shows that the nature of the flow behind this cavity is complex and highly unsteady.

Figure 4.5 shows the mean velocity field and vorticity field for a base model fitted with the 1/3 h cavity. The mean flow is symmetric with respect to the X-Z plane at Y = 0 . In the reverse flow region, the maximum upstream velocity is approximately 24% of the free stream velocity.

Figure 4.6 shows the mean flow streamlines in the near wake of the 1/3 h cavity at vertical plane at Y = 0. It is inferred from this figure that the length of the recirculation region is around 42 mm. Similar to the base model, there are two circulatory regions in which the flow rotates in direction opposite to each other. The recirculation regions formed are symmetric with respect to the center wake line. The length of the recirculation region is not changed much with the attachment of the 1/3 h cavity to the base model, but the area of the recirculation region decreased compared to the base model.

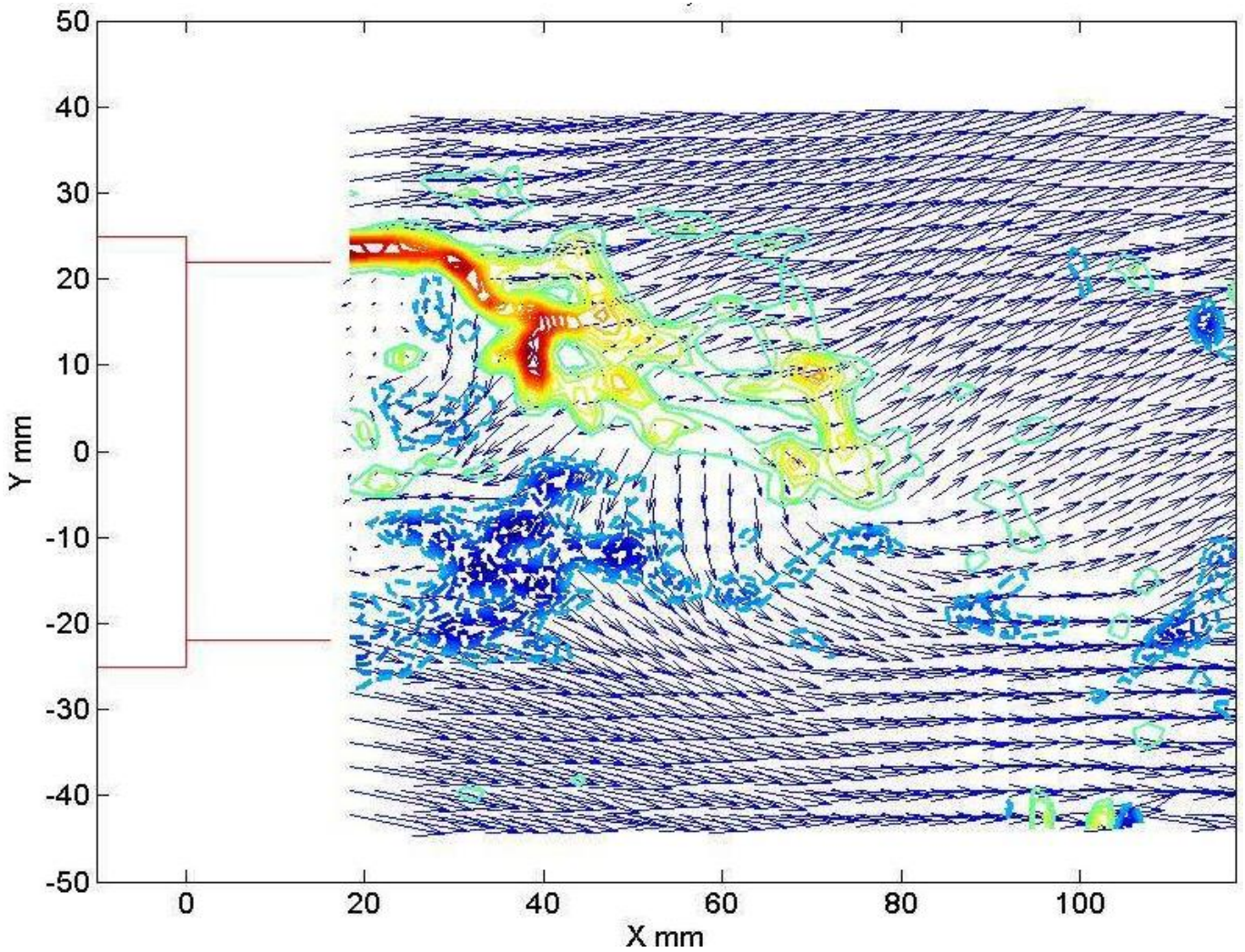

Figure 4.4 Instantaneous velocity and vorticity fields in the symmetry plane of the base model fitted with 1/3 h cavity.

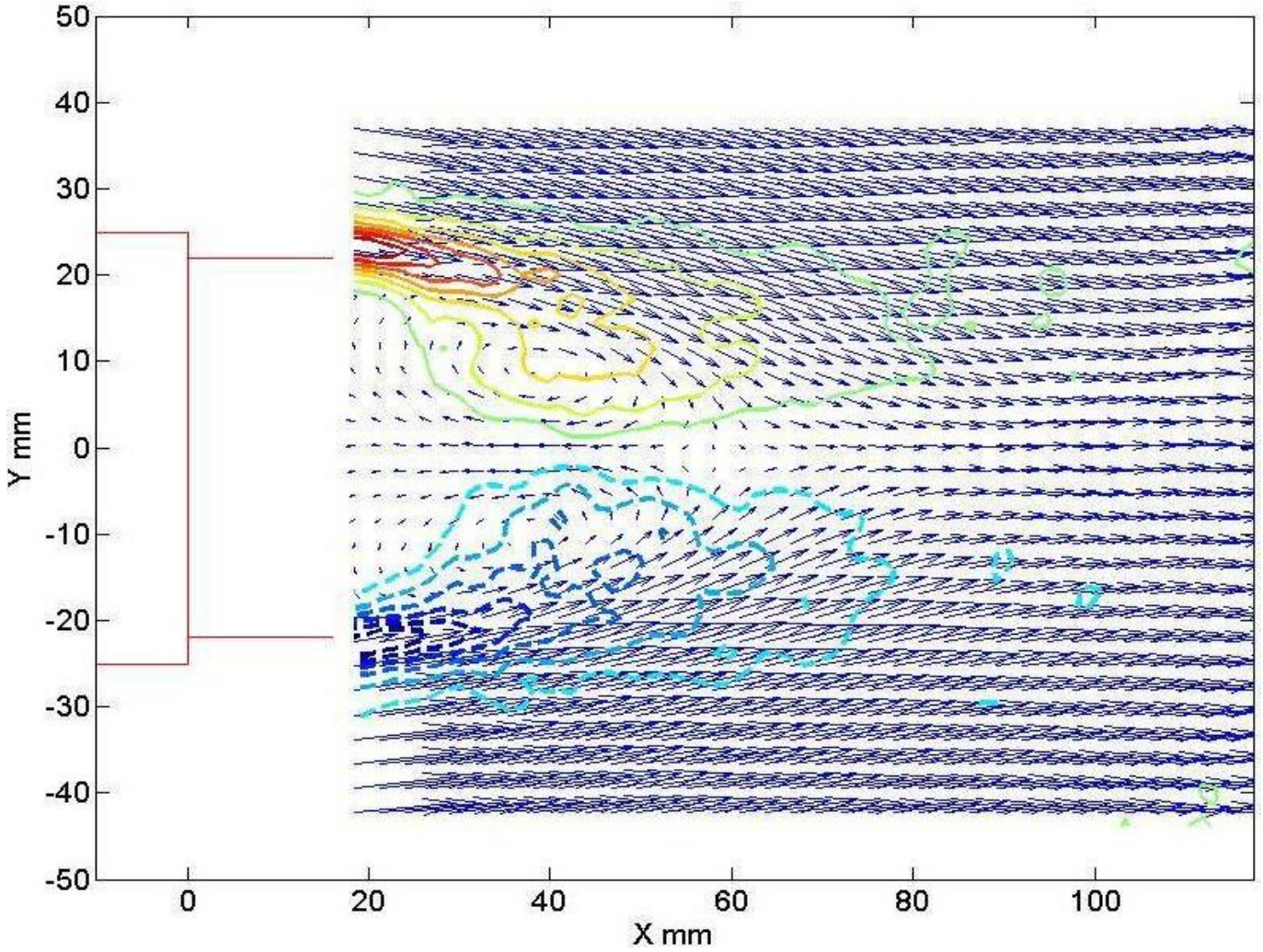

Figure 4.5 Mean velocity and vorticity fields in the symmetry plane of the base model fitted with 1/3 h cavity.

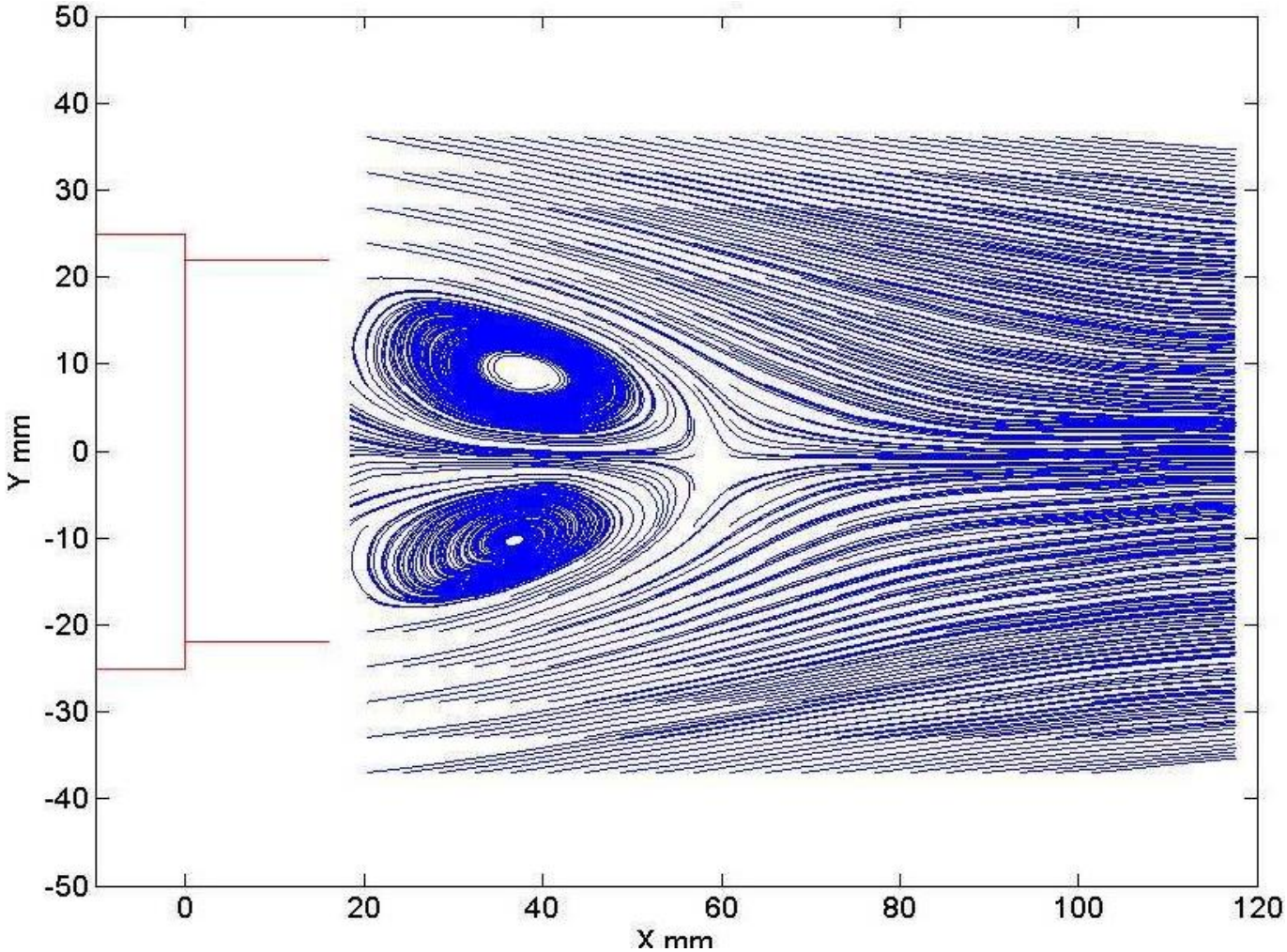

Figure 4.6 Streamlines of the mean velocity field in the symmetry plane of the base model fitted with 1/3 h cavity.

4.1.3 Base model fitted with 2/3 h cavity

Figure 4.7 shows a typical instantaneous vector flow field measured in the vertical plane (Z = 0) of the base model fitted with the 2/3 h cavity. Similar to the 1/3 h cavity, the upper and lower shear layers originate from the cavity edges. This figure shows smaller recirculation region behind the cavity. Near the cavity, the velocity of the reverse flow entering the cavity is smaller than in the near wake.

Figure 4.8 shows the mean velocity field and vorticity field for a base model fitted with the 2/3 h cavity. The mean flow is symmetric with respect to the geometrical symmetry plane (X-Z plane at Y = 0) as observed in previous cases. In the reverse flow region the maximum upstream velocity (i.e. the flow in the reverse direction) is approximately 21% of the free stream velocity.

Figure 4.9 shows the mean flow streamlines at the symmetry plane (Y = 0). It is inferred from the figure that length of the recirculation region is around 42 mm. The length of the recirculation region is not changed much, when the 2/3 h cavity is attached to the base model, but the area of the circulation region decreased with respect to the base model.

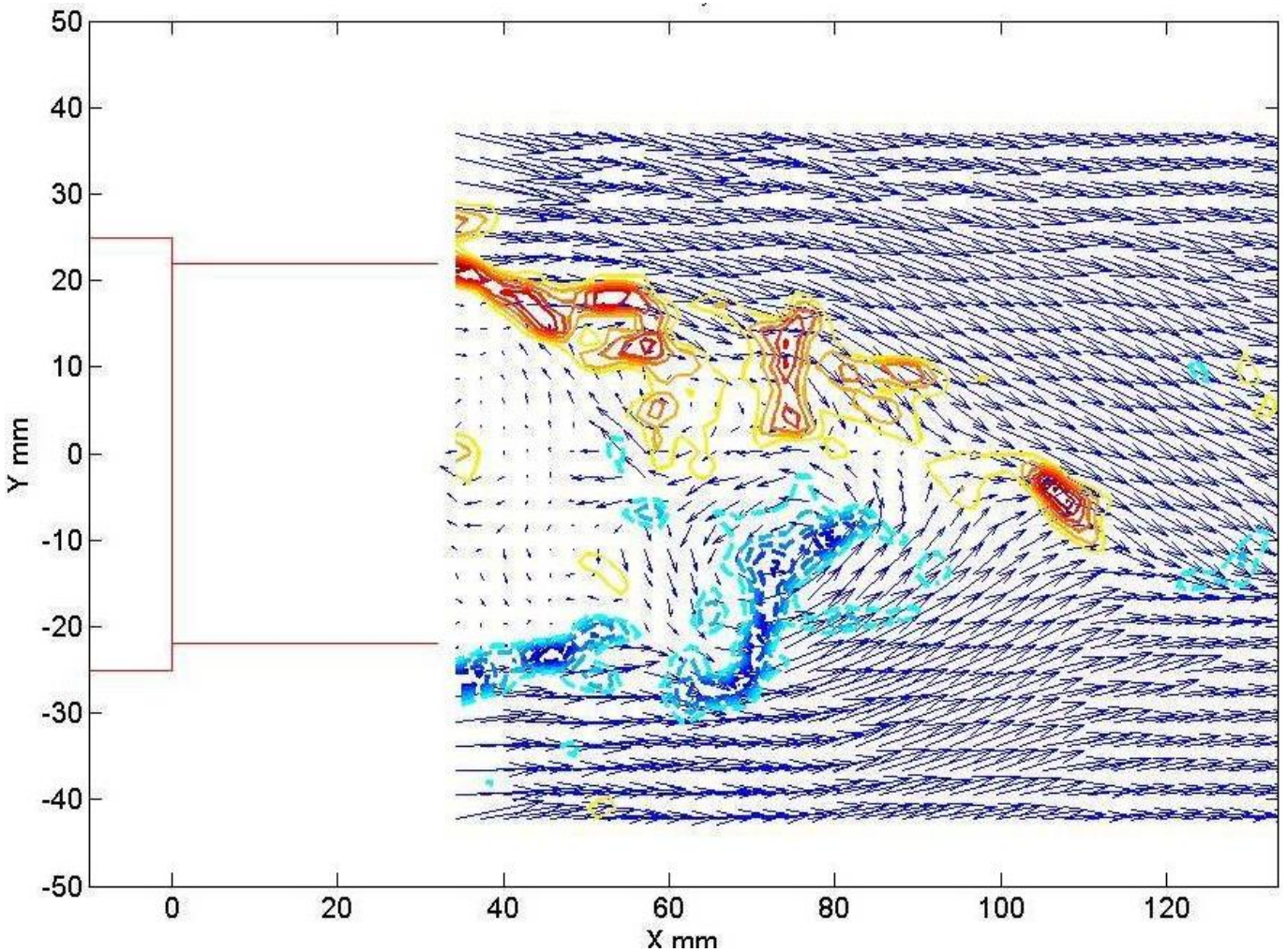

Figure 4.7 Instantaneous velocity and vorticity fields in the symmetry plane of the base model fitted with 2/3 h cavity.

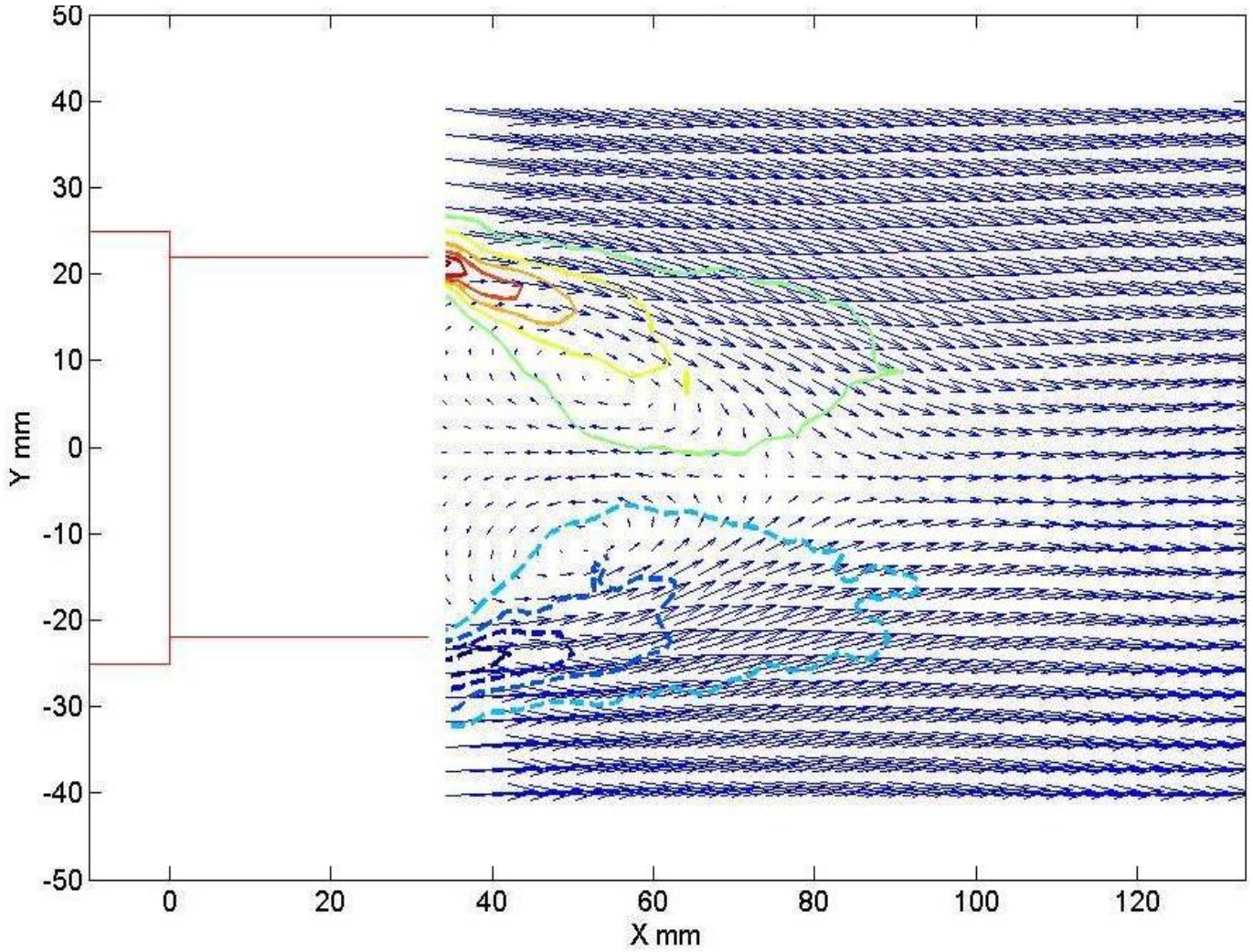

Figure 4.8 Mean velocity and vorticity fields in the symmetry plane of the base model fitted with 2/3 h cavity.

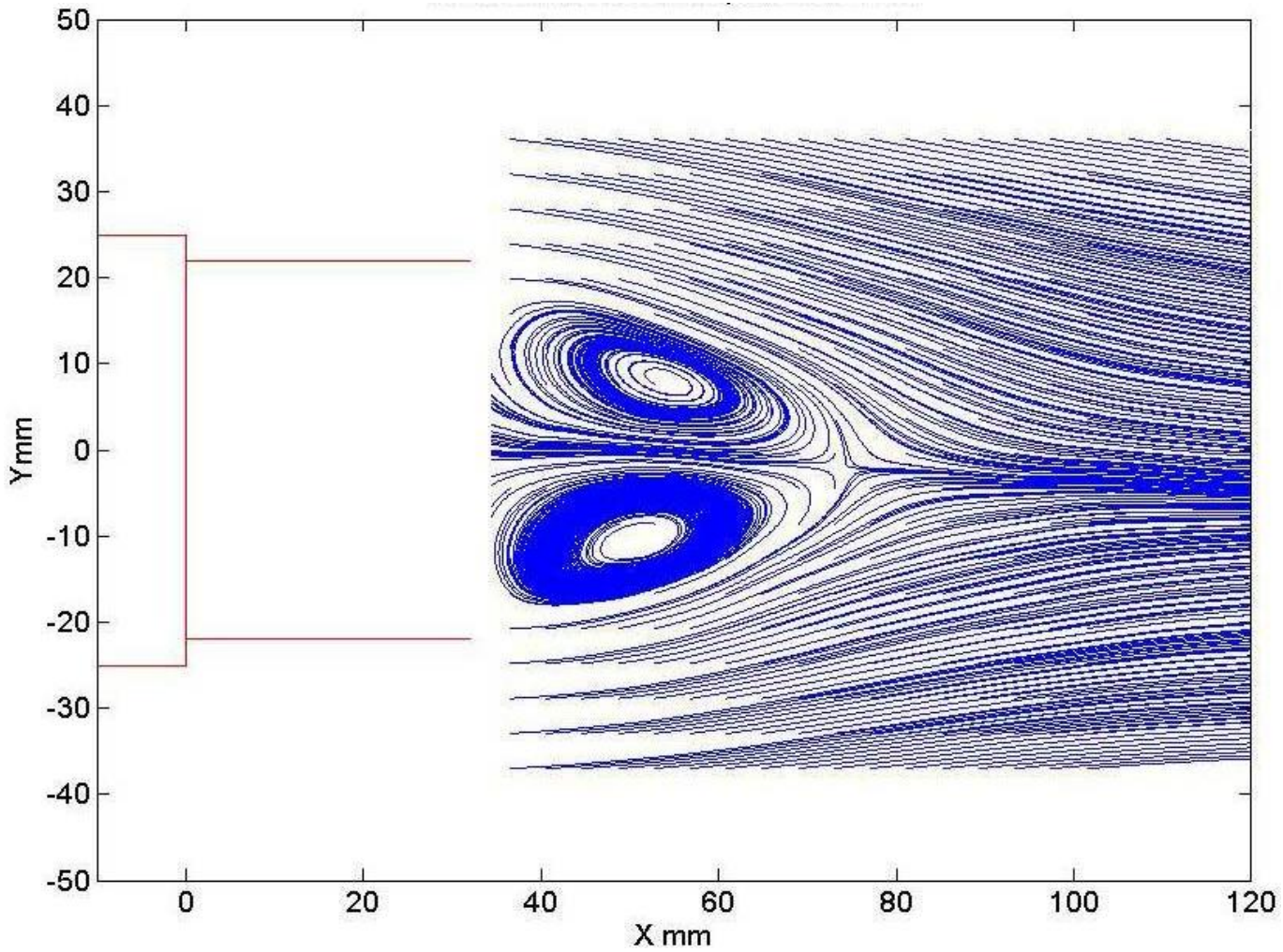

Figure 4.9 Streamlines of the mean velocity field in the symmetry plane of the base model fitted with 2/3 h cavity.

4.1.4 Base model fitted with angled cavity

Figure 4.10 shows a typical instantaneous velocity vector flow field. There is a reverse flow region that gets developed behind the model, and it tends to circulate in the vicinity of the cavity. Again this figure shows the nature of the flow behind this cavity, which is complex and highly unsteady.

Figure 4.11 shown below is a plot of the mean velocity field and vorticity field for a base model fitted with angled cavity. As for previous cases, the mean flow is symmetric with respect to the geometrical symmetry plane (X-Z plane at Y = 0). In the recirculation region, the maximum upstream velocity is approximately 19% of the free stream velocity.

Figure 4.12 illustrates the mean streamlines of the flow at the symmetry plane. This figure shows two circulatory regions in which the flows rotates in opposite directions. It is inferred from this figure that the length of the recirculation region is around 40 mm. The recirculation regions formed are symmetric with respect to the center wake line as found for previous arrangements.

The area of the circulation region when the angled cavity is attached to the base model is slightly more than that of the 1/3 h and 2/3 h cavities but less than that of the base model.

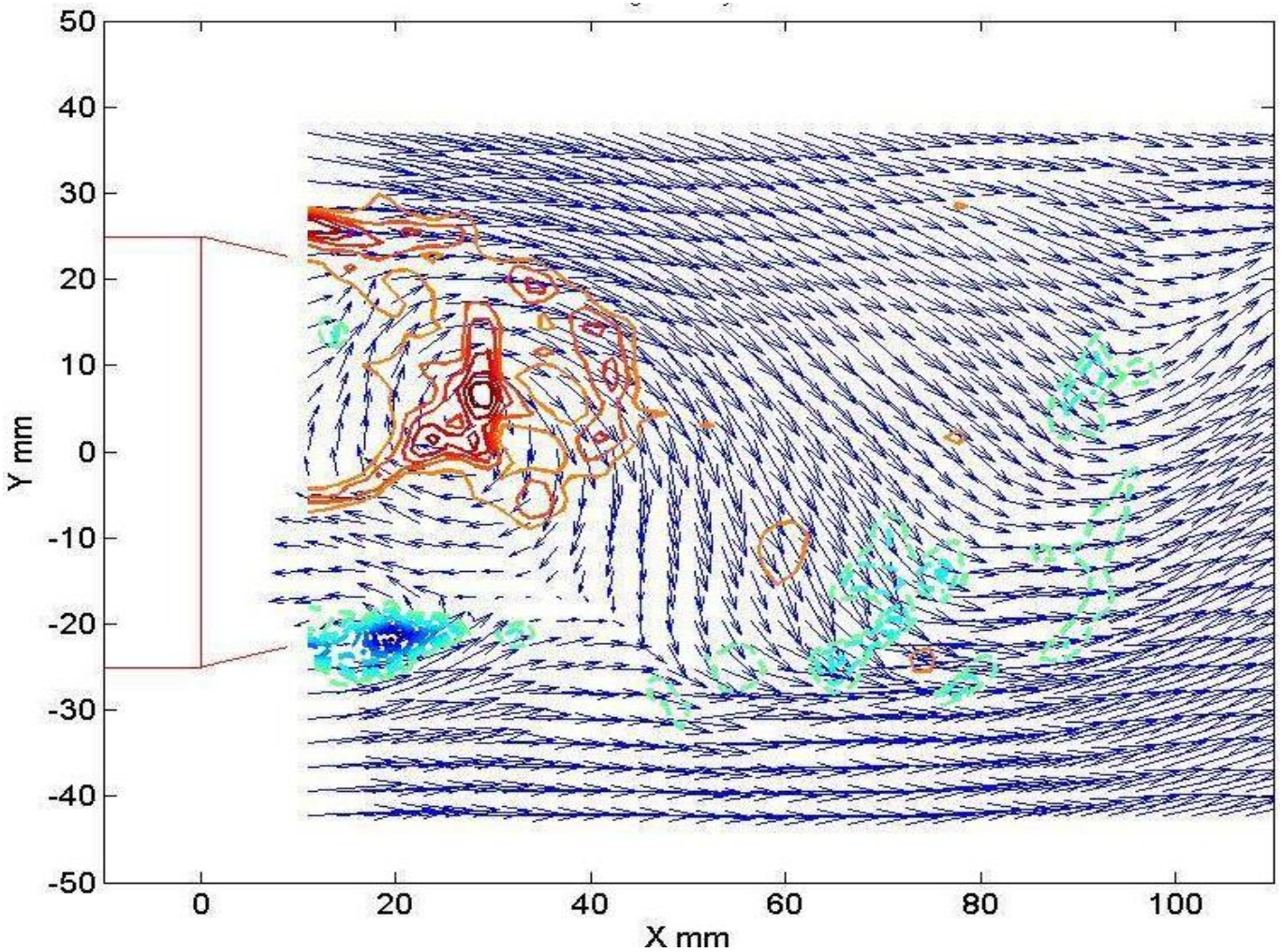

Figure 4.10 Instantaneous velocity and vorticity fields in the symmetry plane of the base model fitted with angled cavity.

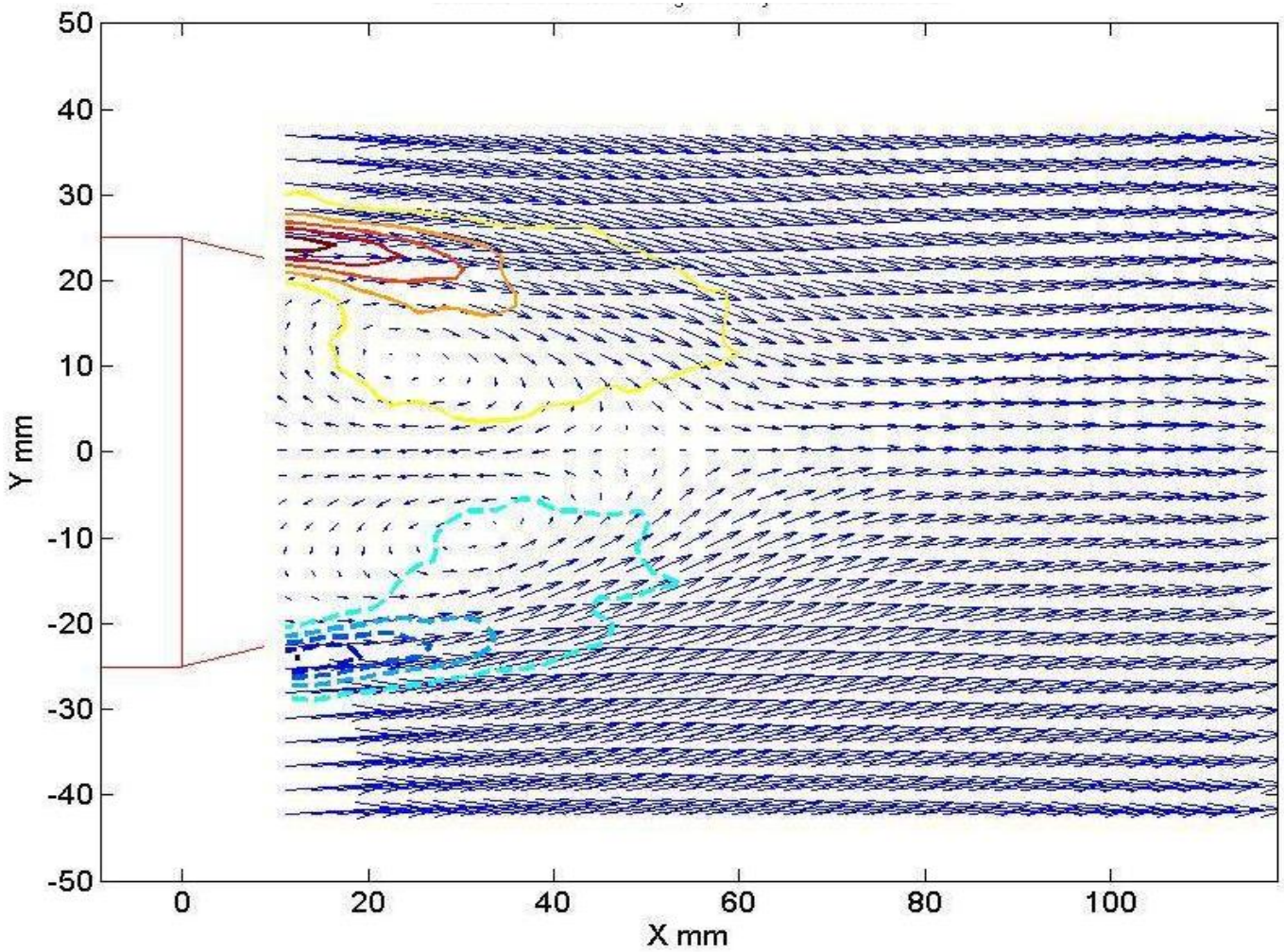

Figure 4.11 Mean velocity and vorticity fields in the symmetry plane of the base model fitted with angled cavity.

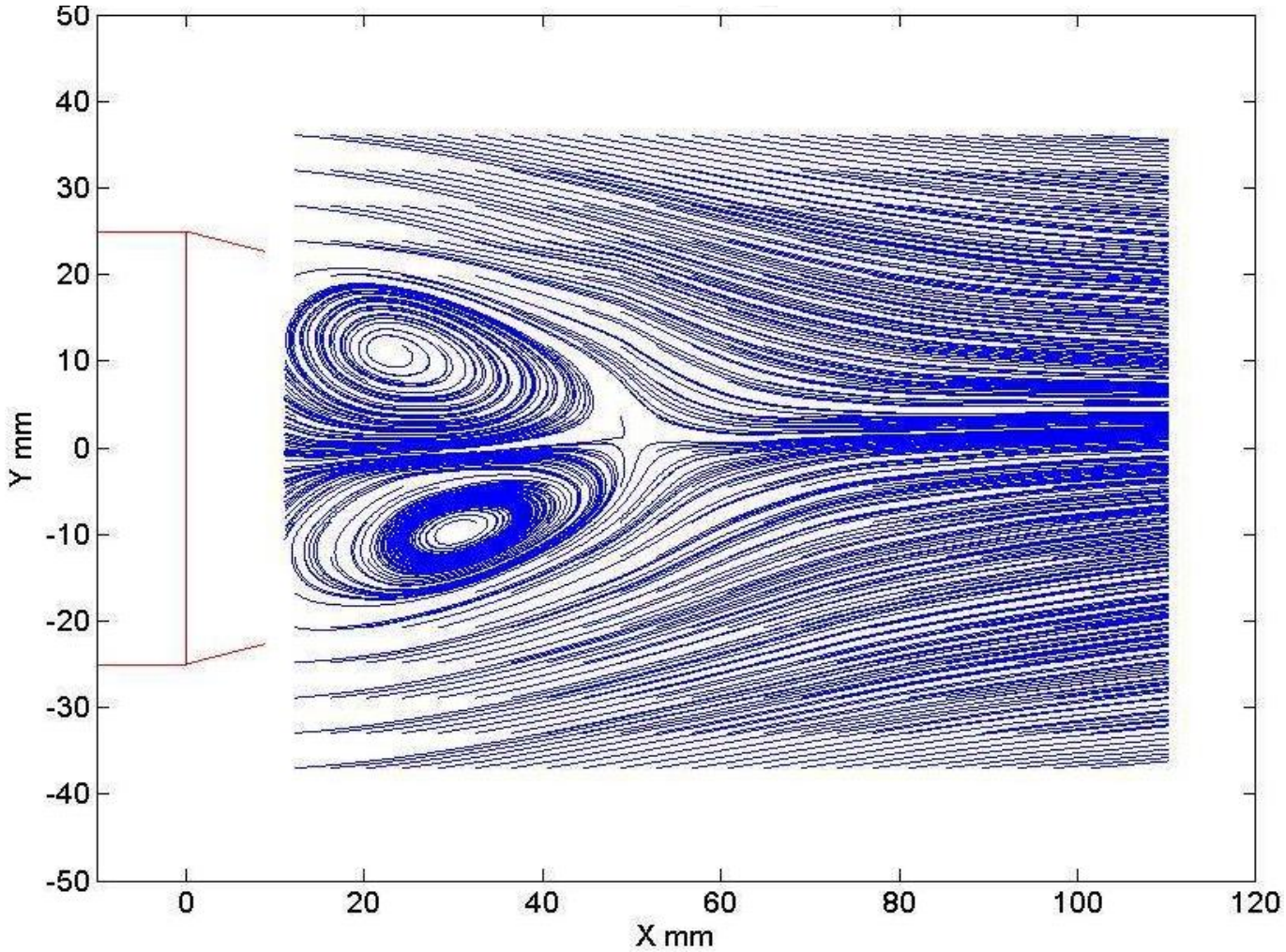

Figure 4.12 Streamlines of the mean velocity field in the symmetry plane of the base model fitted with angled cavity.

4.2 Mean Velocity Profiles

4.2.1 Base model

Figure 4.13 shows the mean streamwise and vertical velocity components in the symmetry plane of the near wake of the base model at four downstream locations of the base model, namely at x = 25, 50, 75, 100 mm. Figure 4.13 (a) shows the streamwise mean velocity component. This figure indicates that the flow is symmetric about the centre wake line (Y = 0). There is a reversed flow region between x ~ 10 mm and 45 mm. The maximum reverse flow velocity in the recirculation region is around 26 % of the free stream velocity. Also, it is noted that the downstream evolution shows a reduction of the maximum velocity as the shear layer width increases.

Figure 4.13 (b) shows the mean vertical velocity component at the symmetry plane. The figure shows that the vertical velocity is large near the base of the model, due to separation, but decreases as the flow evolves downstream. The maximum mean vertical velocity (v_m) obtained in the near the wake of the model is around 20% of the freestream velocity.

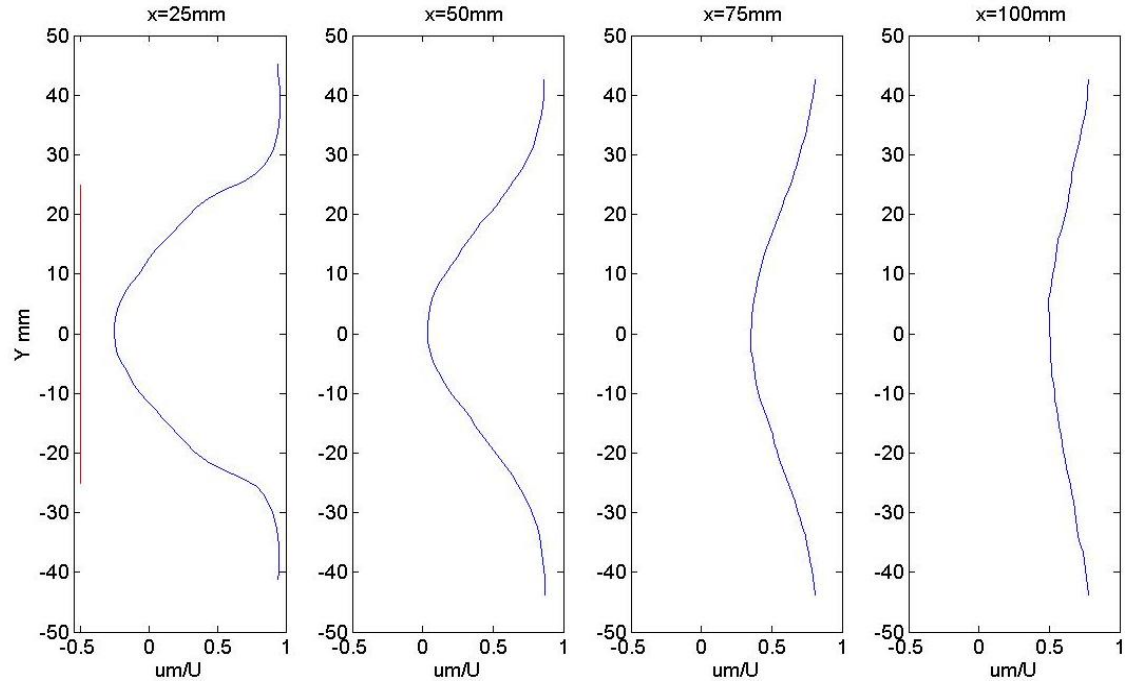

(a)

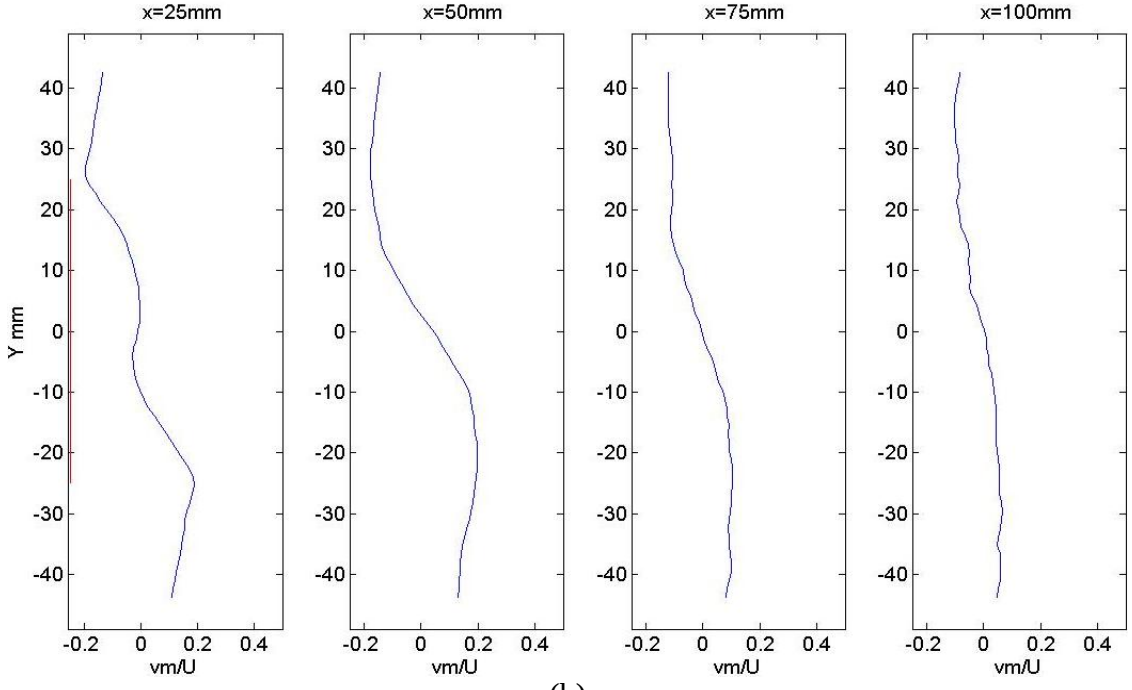

(b)

Figure 4.13 Mean velocity profiles of the flow in the symmetry plane of the wake of the base model: (a) streamwise velocity component; (b) vertical velocity component.

4.2.2 Base model fitted with 1/3 h cavity

Figure 4.14 shows the mean streamwise and vertical velocity components in the symmetry plane of the near wake of the base model fitted with the 1/3 h cavity at four downstream locations at x = 25, 50, 75 and 100 mm downstream the cavity.

Figure 4.14(a) shows the streamwise mean velocity component. This figure indicates that the flow is symmetric about the centre wake line, i.e. at Y = 0. Note that the near wake is shifted by 16 mm (length of the cavity) when fitted with the 1/3 h cavity. There is a reverse flow region between x ~ 18 mm and 58 mm. The curves in the plots are similar to that of figure 4.13 (a) and no major changes are seen in the curve pattern. The maximum upstream velocity in the near wake of the cavity is approximately 24% of the free stream velocity. The figure also shows that the thickness of the velocity deficit behind this cavity is smaller than behind the base model. Figure 4.14 (b) shows the mean vertical velocity profiles at the same plane and a similar trend to that in figure 4.13 (b). The maximum mean vertical velocity (v_m) obtained in the near the wake of the model is around 14% of the freestream velocity.

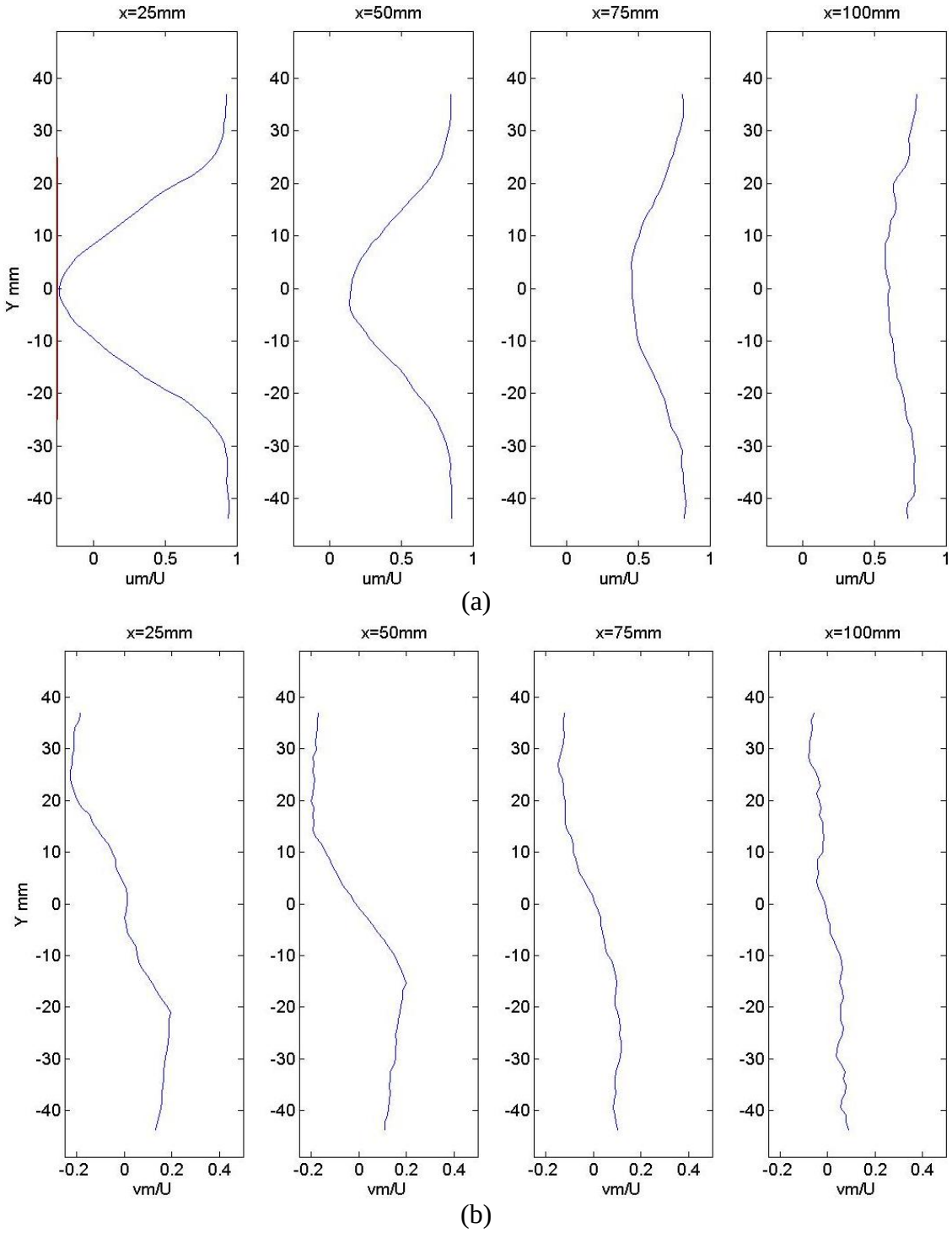

Figure 4.14 Mean velocity profiles of the flow in the symmetry plane of the wake of the base model fitted with 1/3 h cavity: (a) streamwise velocity component; (b) vertical velocity component.

4.2.3 Base model fitted with 2/3 h cavity

Figure 4.15 shows the mean streamwise and vertical velocity components in the symmetry plane of the near wake of the base model fitted with the 2/3 h cavity. Figure 4.15 (a) shows the streamwise mean velocity component at several downstream locations (x = 25, 50, 75 and 100 mm). Note that the near wake is shifted by 32 mm when fitted with the 2/3 h cavity. There is a reversed flow region between x ~ 35 mm and 72 mm. The maximum upstream velocity is around 21% of the free stream velocity.

Figure 4.15 (b) shows the mean vertical velocity component at the symmetry plane. Similar to Figure 4.13 (b), the vertical velocity is higher near the cavity but decreases as the flow evolves downstream. The maximum vertical velocity (v_m) obtained is 15% of the free stream velocity. There is no significant change in the curve pattern as compared to Figures 4.13 (b) and 4.14 (b).

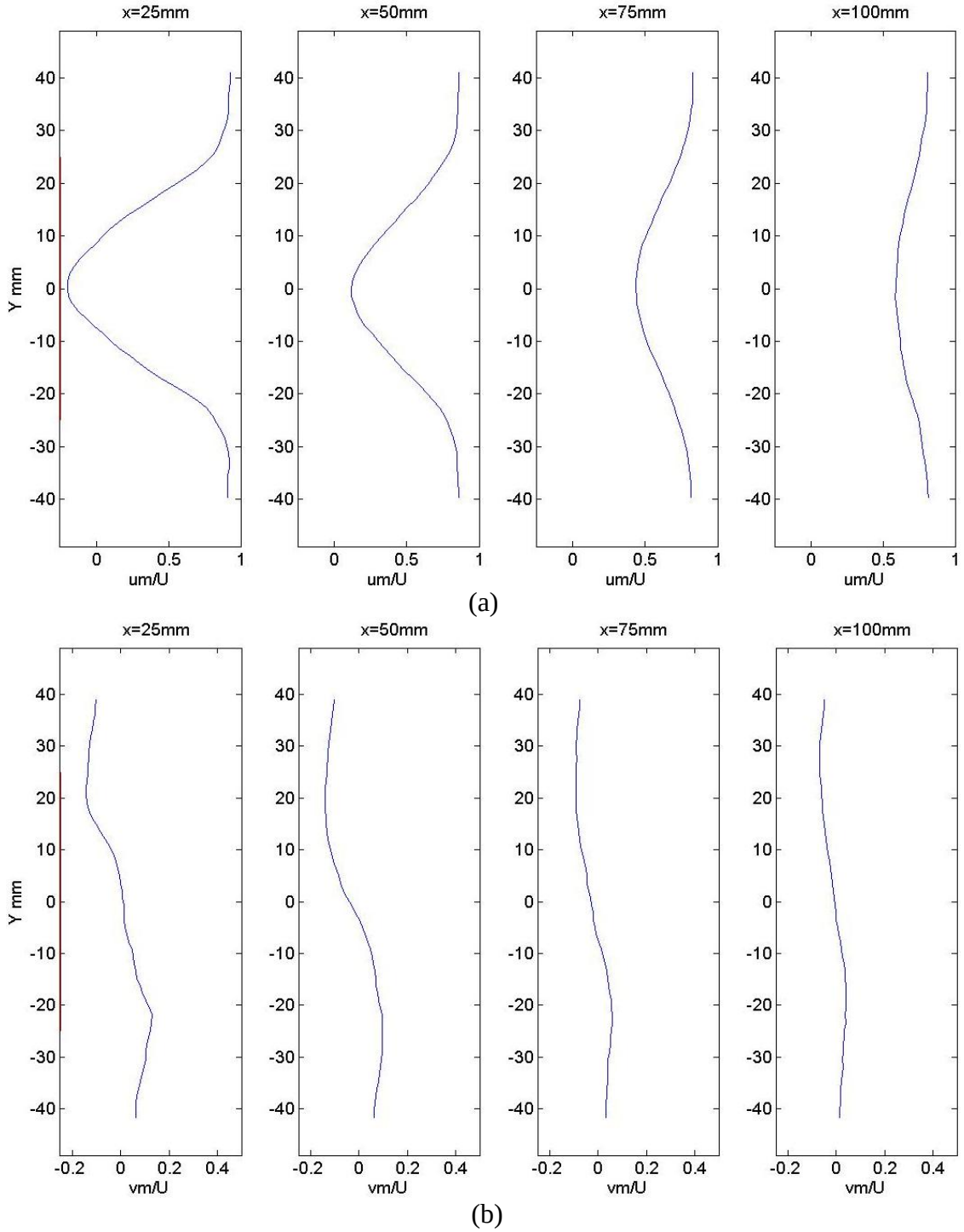

Figure 4.15 Mean velocity profiles of the flow in the symmetry plane of the wake of the base model fitted with 2/3 h cavity: (a) streamwise velocity component; (b) vertical velocity component.

4.2.4 Base model fitted with angled cavity

Figure 4.16 shows the mean velocity component in the symmetry plane of the near wake of the base model fitted with angled cavity at four downstream locations of the base model (x = 25, 50, 75 and 100 mm). Figure 4.16 (a) shows the streamwise mean velocity component, and it indicates that the flow is symmetric about the centre wake line (Y=0). Note that the near wake is shifted by 8.7 mm (length of the cavity) compared to the base model when fitted with the angled cavity. There is a reversed flow region between x ~ 10 mm and 50 mm. The maximum upstream velocity is around 19% of the freestream velocity.

Figure 4.16 (b) shows the mean vertical velocity profiles in the symmetry plane at the same streamwise locations. There is no significant change in the trend as compared to Figures 4.13 (b), 4.14 (b) and 4.15 (b). The maximum vertical velocity (v_m) obtained is 22% of the free stream velocity.

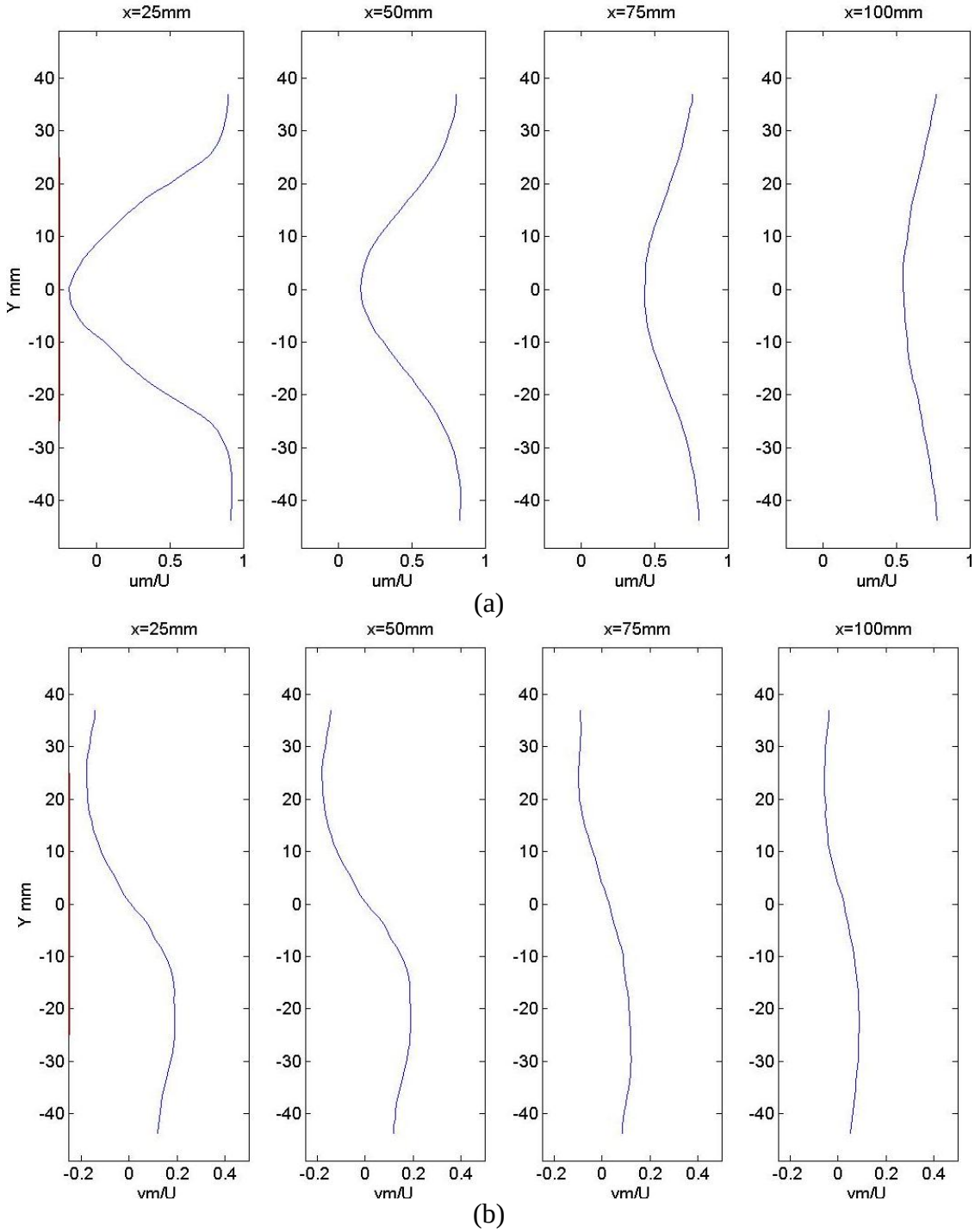

Figure 4.16 Mean velocity profiles of the flow in the symmetry plane of the wake of the base model fitted with angled cavity: (a) streamwise velocity component; (b) vertical velocity component.

CHAPTER 5

CONCLUSIONS AND RECOMMENDATIONS

5.1 Conclusions:

An experimental investigation was conducted for an elliptical bluff body with a blunt base. The objectives of this study are

- To determine how the different cavities affect the base pressure and drag of a two-dimensional bluff body.
- To study the effects of the best drag reduction devices on the vortex shedding phenomenon behind the base model.
- To study the near wake flow structure behind the model and cavities arrangement.

The measurements were conducted at a Reynolds number of $2.6x10^4$ based on the height of the body (h = 50 mm). The steady base pressure results show that the base pressure coefficient for the base model was around -0.58, which agrees well with the results of Bearman [1], [28] and Park [8]. By attaching the cavities, the base pressure was increased. The increase in base pressure coefficient was 10%, 46%, 26.5% and 20% for 1/6 h cavity, 1/3 h cavity, 2/3 h cavity and angled cavity, respectively.

The attachment of the cavities to the base model did not change

the vortex shedding frequency (~ 11Hz) and hence the Strouhal number (~ 0.07), but there is a significant increase in the energy of the peak, when cavities were attached to the base model, and this agrees well with the results of Lanser [42] and Morel [3].

The drag force acting on the base model alone and with the attachment of the cavities were obtained by using the momentum integral method. The drag coefficient of the base model was around 0.58. The largest drag reduction was obtained with the 1/3 h cavity (C_d ~ 0.35), followed by 2/3 h cavity (C_d ~ 0.43), angled cavity (C_d ~ 0.48), 1/6 h cavity (C_d ~ 0.52) and finally the closed-C cavity (C_d ~ 0.54). Comparing the percentage changes in the drag and base pressure coefficients, it is clear that the drag coefficient is almost equivalent to base pressure for a two-dimensional body. This has been verified in many

studies (Nash [27, 36], Park [8] and Viswanath [30].

Nash [27, 36] got a 20% reduction in base drag when he used a square cavity for a 2-dimensional bluff body model which has single-wedged shaped forebody (8.6^{o} total included angle, approximately) at Mach numbers ranging from 0.2 to 0.4. The maximum base drag reduction obtained for the same elliptical bluff body in the literature was by Park et al [8] which was from 30 to 33%, by using staggered tabs at the base of the body.

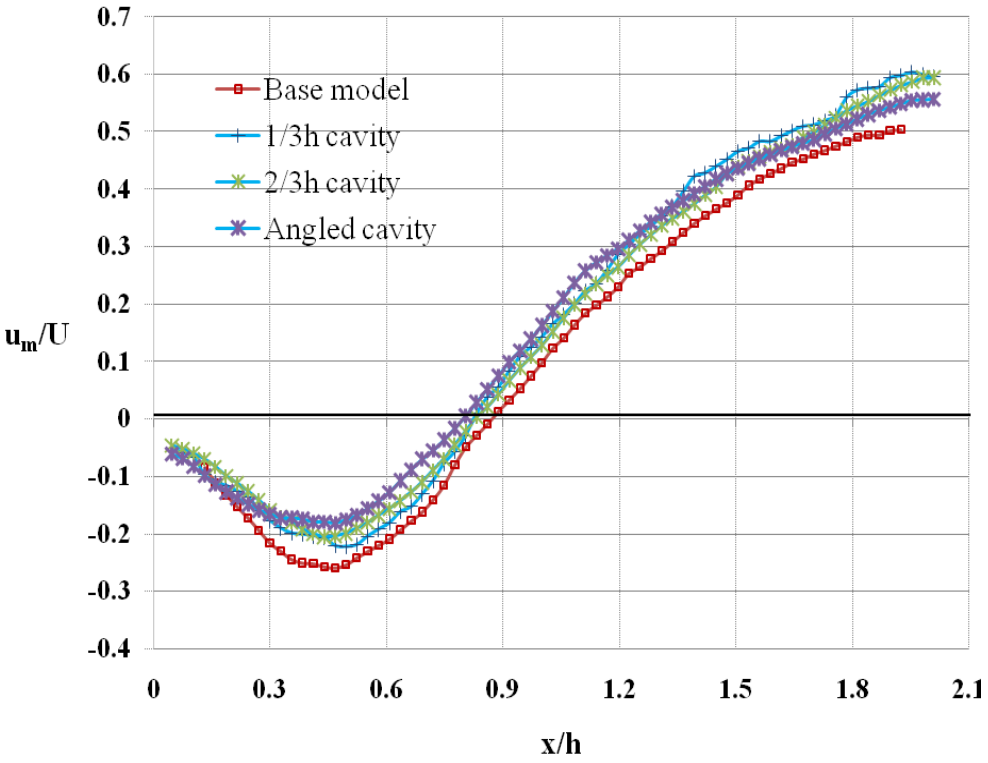

Figure 5.1 Mean velocity variation with downstream distance along the center of the wake for the base model, 1/3 h, 2/3 h and angled cavities.

Figure 5.1 shows the velocity variation with downstream distance along the center of the wake for the base model, 1/3 h, 2/3 h and angled cavities. From this figure, the length of the recirculation region (x_R) is obtained by calculating the distance between the points from

where the curve originates to the point where the curve crosses the axis ($u_m/U = 0$), where u_m is the mean streamwise velocity and U is the free stream velocity. The length of the recirculation region for the base model is around 48 mm i.e. almost equivalent to base model height. For the 1/3 h cavity, 2/3 h cavity and angled cavity, the length of the recirculation region (x_R) is around 42mm, 42mm and 40mm respectively. From this figure, it is inferred that the length of the recirculation region (x_R) for the cavities decrease slightly when cavities are fitted to the base model. Also the recirculation region length (x_R) of the two cavities (1/3 h and 2/3 h cavities) is more or less of same value.

5.2 Recommendations :

- More cavities of different shapes (such as multi-stepped cavity, different length open cavities and angled cavities of other different angles) can be tested for base drag and wake properties for the same two-dimensional bluff bodies.
- The vortex shedding can be studied by measuring the shedding frequency in the shear layer by using a hot-wire anemometer to compare the results with those in the literature.
- Active forcing (blowing and suction) can be done together with the cavities along the span of the bluff body model to break down the vortices and to enhance the mixing of the shear layers in the near wake.

REFERENCES

[1] Tombazis, N. and Bearman, P.W., "A study of three-dimensional aspects of vortex shedding from a bluff body with a mild geometric disturbance", *Journal of Fluid Mechanics*, 1997, Volume 330, pp. 85-112.

[2] Sovran, G., Morel, T., and Wason, W.T., Jr., "Aerodynamic drag mechanisms of bluff bodies and road vehicles", *General Motors Research Laboratories* 1978.

[3] Morel, T., " Effect of base cavities on the aerodynamic drag of an axisymmetric cylinder", *Aeronautical Quarterly*, 1979. Vol. 30, part 2, pp 400-412.

[4] Freund, J.B. and Mungal, M.G., "Drag and wake modification of axisymmetric Bluff bodies using Coanda blowing", *Journal of Aircraft*, May-June 1994, Volume 31, No.3, pp 572-578.

[5] Koenig, Keith.C., Bridges, G.T. and David, H., "Transonic flow modes of an axisymmetric blunt body", *AIAA*, USAF-supported research, July 25-28, 1988, pp7.

[6] Hucho, W., and Sovran G., "Aerodynamics of road vehicles" *Annual Review of Fluid* Mechanics, January 1993, Volume 25, pp 485-537.

[7] Mair, W.A., "Reduction of base drag by boat-tailed after bodies in low speed flow", *Aeronautical Quarterly, 1969, Volume 20, pp 307-320.*

[8] Park, H., Kim, Ju., Hahn, S., Kim, Je., Lee, D.K., Choi, J., Jeon, W.P. and Choi, H., "Drag reduction in flow over a two-dimensional bluff body with a blunt trailing edge using a new passive device", *Journal of Fluid Mechanics*, 2006, Volume.563, pp.389-414.

[9] Wood, C.J., "The effect of base bleed on a periodic wake", *Journal of Royal Aeronautical Society*, 1964, Volume 68, pp 477.

[10] Yao, Y.F., Thomas, T. G., Sandham, N. D., and Williams, J. J. R., "Direct numerical simulation of turbulent flow over a rectangular trailing edge", *Theoretical Computational Fluid Dynamics.* 2001, Volume 14, pp 337.

[11] Tanner, M., "A method of reducing the base drag of wings with blunt trailing edges", *Aeronautical Quarterly*, 1972, Volume 23, pp 15.

[12] Petrusma, M.S. and Gai, S. L., "The effect of geometry on the base pressure recovery of the segmented blunt trailing edge", *Aeronautical Journal*, 1994, Volume 98, pp 267.

[13] Bearman, P.W., "The effect of base bleed on the flow behind a two-dimensional model with a blunt trailing edge", *Aeronautical Quarterly*, 1967,Volume 18, pp 207.

[14] Kim, Ju., Hahn, S., Kim, Je., Lee, D.K., Choi, J., Jeon, W.P., and Choi, H., "Active control of turbulent flow over a model vehicle for drag reduction*", Journal of Turbulence*, 2004, Volume 5:1, pp112.

[15] Hoerner, S.F., "Base drag and thick trailing edges", *Journal of Aerospace Sciences* October, 1950, Volume 17, pp 622.

[16] Hoerner, S.F., "Fluid -dynamic drag", Book, 1958.

[17]Roshko, A., "On the wake and drag of bluff bodies", *Journal of Aerospace Sciences* February, 1955, Volume 22, pp 124.

[18] Roshko, A., "On the drag and shedding frequency of two-dimensional bluff bodies", *N.A.C.A. Tech Note 3169*. July, 1954.

[19] Mair, W.A., "The effect of a rear-mounted disc on the drag of a blunt-based body of revolution", *Aero. Quarterly*, 1965, Volume 16, pages 350-360.

[20] Kentfield, J.A.C., "Drag reduction by means of controlled separated flows", *AIAA*, 1985, pp1800.

[21] Wikoff, D., Cottrell, C.J. and Packard, J.D., "An examination of controlled vortex drag using stepped after bodies from M = 0.5 to 3.0", *AIAA-1987-445 Aerospace Sciences Meeting*, 25th, Reno, NV, Jan 12-15, pp 1987.

[22] Kidd, James. A., "An investigation of drag reduction using stepped after bodies," *AIAA, Aerospace Sciences Meeting*, 9-12. Jan. 1989, Volume 5, pp.1989.

[23] Viswanath, P. R., "Base drag characteristics of multi-step after bodies", *NAL PDEA: 9507*.

[24] Viswanath, P. R. and Patil, S. R., "Drag characteristics of a class of non-axisymmetric after bodies at high speeds", *NAL PD: EA 9407*.1994.

[25] Kruiswyk, R.W. and Dutton, J.C., "Effects of a base cavity on subsonic near-wake flow", *AIAA Journal*, November 1990, Vol.28, No.11, pp 1885-1893.

[26] Nash, J.F., "A review of research on two-dimensional base flow*", Aerodynamics Division, N.P.L*, March, 1962, Reports and Memoranda No. 3323.

[27] Nash, J.F., "A discussion of two-dimensional turbulent base flows", July, 1965**,** Reports and Memoranda No. 3468.

[28] Bearman, P.W., " Investigation of the flow behind a two-dimensional model with a blunt trailing edge and fitted with splitter plates", *Journal of Fluid Mechanics*,1965,Volume.21, pp.241.

[29] Molezzi, M.J. and Dutton, J.C., "Study of subsonic base cavity flow field structure using Particle Image Velocimetry", *AIAA Journal*, November 1990, Volume.33, No.2, pp 201-209.

[30] Viswanath, P.R., "Flow management techniques for base and afterbody drag reduction", *Prog in Aerospace Sciences* 1996, Volume.32, pages 79-129.

[31] Khalighi, B., Zhang, S., Koromilas, C., Balkanyi, S.R., Bernal, L.P., Iaccarino, G. and Moin, P., "Experimental and computational study of unsteady wake flow behind a bluff body with a drag reduction device", *Society of Automotive Engineers*. Inc. 2001, Volume 1, pp.207.

[32] Mathur, N. B. and Viswanath, P.R., "Drag reduction from Square-Base after bodies at high speeds", *Journal of Aircraft*, July-August 2004, Volume 41, No. 4, pp 811-820.

[33] Grace, S.M., Dewar, W.G and Wroblewski, D.E., "Experimental investigation of the flow characteristics within a shallow wall cavity for both laminar and turbulent upstream boundary layers", *Experiments in Fluids*, 2004, Volume 36, pages 791-804.

[34] Cooper, K.R., "The effect of front-edge rounding and rear-edge shaping on the aerodynamic drag of bluff vehicles in ground proximity", *SAE Technical Paper Series*, February 25-March 1,1985,pp 1-32.

[35] Frank, M.White., "Viscous Fluid Flow", University of Rhode Island, 1992.

[36] Nash, J.F, Quincey, V.G. and Callinan, J., "Experiments on two-dimensional base flow at subsonic and transonic speeds ", January, 1963**,** Reports and Memoranda No. 3427.

[37] Park, H., Choi, H., Jeon, W.P. and Jung, Y.Y., "Mixing enhancement behind a backward-facing step using tabs", *Physics of Fluids*, October 2007, Volume 19, pages 1-12.

[38] Pastoor, M., Henning, L., Noack, B. R., King, R., Tadmor, G., "Feedback shear layer control for bluff body drag reduction ", *Journal of Fluid Mechanics*, August 2008, Volume 608, pages 161-196.

[39] Cai, J., Chng, T.L. and Tsai, H.M., "On vortical flows shedding from a bluff body with a wavy trailing edge", *Physics of Fluids*, June 2008, Volume 20, pages 1-13.

[40] Beaudoin, J.F., Aider, J.L., "Drag and lift reduction of a 3-D bluff body using flaps", *Experiment in Fluids*, 26 February 2008, Volume 44, pages 491–501.

[41] Falchi, M., Provenzano, G. and Pietrogiacomi, D., "Experimental and numerical investigation of flow control on bluff bodies by passive ventilation", *Experiment in Fluids*, 14 April 2006, Volume 41, pages 21–33.

[42] Lanser, R.W., James, C.R. and Kaufman, E.A., "Aerodynamic performance of a drag reduction device on a full-scale tractor/trailer", *SAE Technical Paper Series*, September 23-26, 1991, pages 1-9.

[43] Balkanyi, S.R., Bernal, L.P., Khalighi, B., Zhang, S., Koromilas, C., Iaccarino, G., Moin, P. and Sumantran, V., "Dynamics of manipulated bluff body wakes", *AIAA*, 19-22 June 2000, pages 1-12.

[44] Duell, G.E., and George, A.R., "Experimental Study of a ground vehicle body unsteady near wake", *SAE Technical Paper Series*, March 1-4, 1999, pages 1-14.

[45] Berger, E., Scholz, D. and Schumm, M., "Coherent vortex structures in the wake of a sphere and a circular disk at rest and under forced vibrations", *Journal of Fluids And Structures*, Volume 4, 1990, pages 231-257.

[46] Al-Garni, M. A., Bernal, L.P., Khalighi, B., "Experimental investigation of the flow around a generic SUV," *SAE Paper* 2004-01-0228.

[47] Wu, J.S. and Faeth, G. M., "Sphere Wakes at Moderate Reynolds Numbers in a Turbulent Environment" *AIAA Journal*, Volume 32, No. 3, 1994 pages 535-541.

[48] Abdullah M.Al-Garni, Ahmed Z.Al-Garni and Abdurrahman Aravind., "Experimental Investigation of the effect of Base Cavities on the Base pressure and Wake of a Two-Dimensional Bluff Body" Submitted to *7th IASME/WSEAS conference. on Fluid Mechanics and Aerodynamics (FMA'09)* Moscow, Russia, August 20-22, 2009.

[49] Abdullah M.Al-Garni, Ahmed Z.Al-Garni and Abdurrahman Aravind., "Experimental Investigation of the effect of Base Cavities on the Base drag and Wake of a Two-Dimensional Bluff Body" to be submitted to Journal of Experimental Thermal and Fluid Science.

VITA

- Aravind Chandramohan (Abdurrahmaan).
- Born in Chennai, India.
- Obtained Bachelor's degree with distinction in Mechanical Engineering from University of Madras, in June 2002.
- Completed Master's Degree at King Fahd University of Petroleum & Minerals, Dhahran, Saudi Arabia in April 2009.